Title
Increased Occurrence of Large-Scale Windthrows Across the Amazon Basin

Journal
AGU Advances, 5(6)

ISSN
2576-604X

Authors
Urquiza-Muñoz, J David
Trumbore, Susan
Negrón-Juárez, Robinson I
et al.

Publication Date
2024-12-01

DOI
10.1029/2023av001030

AGU ADVANCING EARTH AND SPACE SCIENCES

AGU Advances

RESEARCH ARTICLE
10.1029/2023AV001030

Increased Occurrence of Large-Scale Windthrows Across the Amazon Basin

J. David Urquiza-Muñoz[1,2,3], Susan Trumbore[1], Robinson I. Negrón-Juárez[4], Yanlei Feng[5], Alexander Brenning[2], C. Michael Vasquez-Parana[3], and Daniel Magnabosco Marra[1,6]

[1]Biogeochemical Processes Department, Max Planck Institute for Biogeochemistry, Jena, Germany, [2]Department of Geography, Friedrich Schiller University Jena, Jena, Germany, [3]Facultad de Ciencias Forestales, Universidad Nacional de la Amazonia Peruana, Iquitos, Peru, [4]Lawrence Berkeley National Laboratory, Berkeley, CA, USA, [5]Department of Civil and Environmental Engineering, Massachusetts Institute of Technology, Cambridge, MA, USA, [6]Julius Kühn Institute (JKI) – Federal Research Centre for Cultivated Plants, Institute for Forest Protection, Braunschweig, Germany

Peer Review The peer review history for this article is available as a PDF in the Supporting Information.

Key Points:

- Windthrows caused by downdrafts associated with convective storms are a natural disturbance that can shape Amazon forests
- A fourfold increase in windthrow frequency from 1985 to 2020 documents an increase in the frequency of damaging convective storms
- Roughly 33% of detected events occurred in only 3% of the Amazon, highlighting regional variation on the impact of large-scale windthrows

Supporting Information:

Supporting Information may be found in the online version of this article.

Correspondence to:

J. D. Urquiza-Muñoz,
jurquiza@bgc-jena.mpg.de

Citation:

Urquiza-Muñoz, J. D., Trumbore, S., Negrón-Juárez, R. I., Feng, Y., Brenning, A., Vasquez-Parana, C. M., & Magnabosco Marra, D. (2024). Increased occurrence of large-scale windthrows across the Amazon basin. *AGU Advances*, *5*, e2023AV001030. https://doi.org/10.1029/2023AV001030

Received 26 AUG 2023
Accepted 12 OCT 2024

Author Contributions:

Conceptualization: J. David Urquiza-Muñoz, Susan Trumbore, Daniel Magnabosco Marra
Data curation: J. David Urquiza-Muñoz, C. Michael Vasquez-Parana
Formal analysis: J. David Urquiza-Muñoz, Susan Trumbore
Funding acquisition: Susan Trumbore

Abstract

Convective storms with strong downdrafts create windthrows: snapped and uprooted trees that locally alter the structure, composition, and carbon balance of forests. Comparing Landsat imagery from subsequent years, we documented temporal and spatial variation in the occurrence of large (≥30 ha) windthrows across the Amazon basin from 1985 to 2020. Over 33 individual years, we detected 3179 large windthrows. Windthrow density was greatest in the central and western Amazon regions, with ∼33% of all events occurring in ∼3% of the monitored area. Return intervals for large windthrows in the same location of these "hotspot" regions are centuries to millennia, while over the rest of the Amazon they are >10,000 years. Our data demonstrate a nearly 4-fold increase in windthrow number and affected area between 1985 (78 windthrows and 6,900 ha) and 2020 (264 events and 32,170 ha), with more events of >500 ha size since 1990. Such extremely large events (>500 ha up to 2,543 ha) are responsible for interannual variation in the overall median (84 ± 5.2 ha; ±95% CI) and mean (147 ± 13 ha) windthrow area, but we did not find significant temporal trends in the size distribution of windthrows with time. Our results document increased damage from convective storms over the past 40 years in the Amazon, filling a gap in temporal records for tropical regions. Our publicly accessible large windthrow database provides a valuable tool for exploring dynamic conditions leading to damaging storms and their ecological impact on Amazon forests.

Plain Language Summary

Windthrows in the Amazon, the uprooting or breaking of trees by winds, are produced by downdrafts associated with strong convective storms. They are a major natural disturbance that can influence the structure, carbon balance and species composition of forests worldwide. Damage by wind can range from single trees to large forest areas, but only windthrow of large enough size can be detected from satellite imagery. We mapped large windthrows (≥30 ha) occurring between 1985 and 2020 in the Amazon to assess possible trends in their spatial and temporal variability. Large windthrows were more common in the central and western Amazon, with ∼33% of all detected events occurring in only ∼3% of the monitored area. Between 1985 and 2020, the number and total area of forests impacted by large-scale windthrows increased about fourfold, suggesting an increase in the number of intense storms that can topple trees although there was no obvious change over time in their spatial or size distribution. We did observe interannual variations in the overall mean size (147 ± 13 ha; 95% CI) reflecting the sporadic contributions from infrequent but very large events (up to 2,543 ha).

1. Introduction

Natural ecological disturbances serve as a record of extreme conditions and exert an important influence on biogeochemical cycles. Windthrows (i.e., trees snapped or uprooted by wind) are an important natural disturbance in the Amazon rainforest (Chambers et al., 2013; Espírito-Santo et al., 2014; Esquivel-Muelbert et al., 2020; Y. Feng, Negrón-Juárez, Chiang, & Chambers, 2023; Feng, Negrón-Juárez, Romps, & Chambers, 2023; Negrón-Juárez et al., 2017; Nelson & Amaral, 1994). They are produced by strong downdrafts associated with convective storms (Garstang et al., 1998; Negrón-Juárez et al., 2018) and thus record the occurrence of such storms and their interaction with the forest. Locally, sufficiently large windthrows trigger forest succession, with new species filling created gaps and leading to changes in structure, diversity and carbon dynamics (Chambers et al., 2009; Marra et al., 2014, 2018; Rifai et al., 2016; Silvério et al., 2019; Urquiza Muñoz et al., 2021). Wind damage can

Investigation: J. David Urquiza-Muñoz, Susan Trumbore, Robinson I. Negrón-Juárez
Methodology: J. David Urquiza-Muñoz, Robinson I. Negrón-Juárez, Alexander Brenning
Resources: Susan Trumbore
Supervision: Susan Trumbore, Alexander Brenning, Daniel Magnabosco Marra
Visualization: J. David Urquiza-Muñoz
Writing – original draft: J. David Urquiza-Muñoz
Writing – review & editing: Susan Trumbore, Robinson I. Negrón-Juárez, Yanlei Feng, Alexander Brenning, Daniel Magnabosco Marra

also impact forests by increasing susceptibility to other disturbances. For example, survivor trees may be more exposed to subsequent wind or other disturbances such as fires (Silvério et al., 2019).

Recent studies have documented that windthrow density is higher in the central and western parts of the Amazon basin, and that they tend to occur more in regions with areas of high mean annual rainfall, lower elevation and higher soil organic matter (Negrón-Juárez et al., 2023). They also overlap with regions having higher values of mean afternoon Convective Available Potential Energy (CAPE) (Y. Feng, Negrón-Juárez, Chiang, & Chambers, 2023; Feng, Negrón-Juárez, Romps, & Chambers, 2023), a measure of the energy available to fuel convection. Climate models predict future increases in storm-favorable conditions (CAPE >1023 J kg^{-1}) and therefore windthrows would be expected to also increase (Y. Feng, Negrón-Juárez, Chiang, & Chambers, 2023; Feng, Negrón-Juárez, Romps, & Chambers, 2023). In addition to their association with damaging winds, strong convective storms are responsible for more than half of the annual rainfall in tropical regions (Negron-Juarez et al., 2024; Schumacher & Rasmussen, 2020), thus changes in their frequency or intensity can also impact forests by affecting hydrology.

A number of lines of evidence point to increases in the intensity of damaging storms over the last 40 years (IPCC report on extremes) (Chen & Dai, 2023), although records documenting such changes are limited in regions like the Amazon Basin, where long-term climate records are sparse. Documentation of the geographical distribution and the size, frequency and severity of windthrows across the Amazon Basin can provide a temporal and spatial history of damage from strong convective storms to compare with other regions. Further, such records can be used to assess the local-to-regional importance of windthrows in terms of their impact on the structure and composition of Amazon forests.

Here, we produce an annual dataset of windthrows occurring across the Amazon basin for 33 years between 1985 and 2020, focusing on describing temporal variations in large wind disturbance. In particular, we assessed (a) the spatial distribution of large (≥30 ha) windthrows across the Amazon basin and whether regions with more clustering of events have shifted with time; (b) temporal changes in windthrow size distribution and severity; and (c) whether there were detectable trends in the occurrence of large windthrows over the last three decades. We evaluated potential explanations for observed interannual variability and temporal trends by comparing them with well-known indicators of climate variability in the Amazon. Our results also identified regions where windthrows occur most frequently and have the greatest potential to influence forest dynamics and composition. Thus the main contribution of this work is the temporal and spatial history of damage from strong convective storms that can be used to inform understanding of strong convection, and the assessment of the importance of windthrows at local-to-regional scales in Amazon forests.

2. Materials and Methods

We used the Google Earth Engine -GEE (Gorelick et al., 2017) platform to perform image analysis and processing, and to identify windthrows across the entire Amazon Basin, encompassing ~700 million hectares. This approach builds on the methods used by Negrón-Juárez et al., 2023 but adds novel aspects: (a) a reliable identification of the year in which detected windthrows occurred; and (b) an improved measurement of the affected area based on shape detection and semi-automatic pixel extraction. A detailed summary of our approach is provided in Figure 1.

2.1. Mapping Windthrows Across the Amazon

2.1.1. Annual Landsat Mosaics

We used Landsat 5 Thematic Mapper (L5) and Landsat 8 Operational Land Imager (OLI8) to create mosaics of images with minimal cloud cover for every year from 1985 to 2020 (example in Figure 2a). We used the Landsat Path/Row World Reference System (WRS-2), which is a global notation used for cataloging Landsat data. The Path/Row is spatially shown as grids, dividing the Amazon into 311 grids (Figure 2a). For each grid we selected the least cloudy scene (<50%), based on image ranking for the dry season of the Amazon (June to December). We used images from June 1 to December 31 to identify windthrows of each target year (e.g., 2005) and compared it with a minimum-cloud scene from the same months in the previous year (in this Case 2004). In some cases where no scene meeting our criteria for maximum cloud cover was found in these months, the period analyzed was locally extended from March 1 to December 31 (See Figure S1a in Supporting Information S1). This procedure is

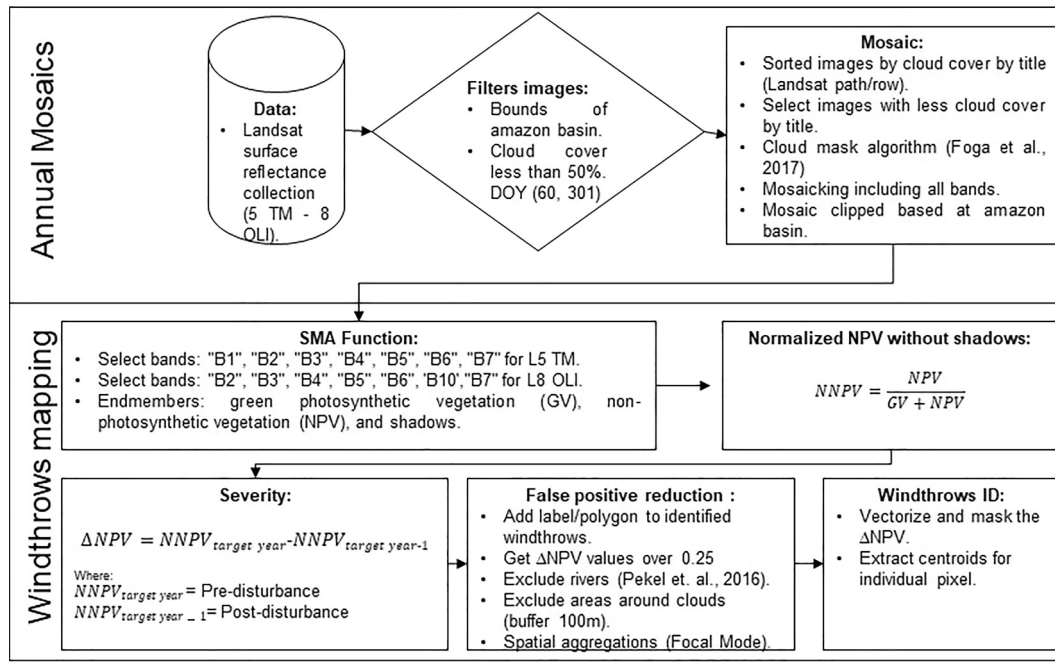

Figure 1. Diagram of windthrow mapping workflows. Construction of the mosaic of images for the Amazon basin (top) and the identification and certification of windthrows (bottom). Confirmed windthrows were manually labeled by enclosing them in a circle of 4 km of radius around the centroid of the windthrow (Figure 2c). These circles were used only to reduce the computational effort when calculating metrics such as windthrow area and severity. The area of the windthrow was determined by counting aggregated pixels with ΔNPV ≥ 0.25 within each polygon, which gave us a reliable estimate of the affected area. This approach is less arbitrary and does not overestimate areas compared to other methods that have used rectangles (Nelson et al., 1994) and triangles (Negrón-Juárez et al., 2023).

justified since the reflectance signal of windthrows remains clear for ∼1 year (Marra et al., 2014; Negrón-Juárez et al., 2011, 2020; Nelson & Amaral, 1994). If several images had the same percentage of cloud cover in a path/row, we selected the recent image in time for that year.

2.1.2. Windthrow Identification

Windthrows were identified by their spectral characteristics, including red coloration due the low radiance in band 4 (L5) and band 5 (OLI8) in a composite image using bands 5, 4, 3 (L5) and 6, 5, 4 (OLI8) (Figure 2c). These features allow us to identify only new events and avoid double counting from year to year. When strong winds impact a forest, they can exert collapsing loads on trees, causing them to fall. The result is often a "fan-shaped" or radiating arrangement of fallen trees spreading from a central point that represents the epicenter of the windthrow event (Nelson et al., 1994). Windthrow tree-mortality is usually higher at the epicenter and decreases toward the edges and within the corridors created by the wind gusts. Windthrows were labeled manually for a reliable identification and each was visually confirmed to avoid false positives. Clouds and rivers were masked out using the CFMask Algorithm (Foga et al., 2017), and the "max extent" band of Global Surface Water Mapping v1.4 (Pekel et al., 2016), respectively. With this approach, we could reliably distinguish windthrows from other types of disturbances, such as deforestation. Further confirmation of events was carried out for selected years when high resolution images in GEE allowed us to see directional alignment of toppled trees in the windthrow.

Confirmation that windthrows occurred in a given year came from comparing features found in the target year (e.g., 1985, 1986 and 1987 up to 2020) with imagery of the previous year (e.g., 1984, 1985 and 1986, up to 2019, respectively). We carried out Spectral Mixture Analysis (SMA) (Adams, 1995) using the "unmix" function available in GEE to identify potential windthrow areas. Linear Spectral unmixing is a standard technique for SMA that is basically a physically-based image-processing tool aiding in precise repeated derivation of quantitative subpixel information (Roberts et al., 1998). It infers the observed spectral signal for a given pixel as a combination of pure spectral signatures, called endmembers (an endmember is the spectral reflectance of a pure surface cover),

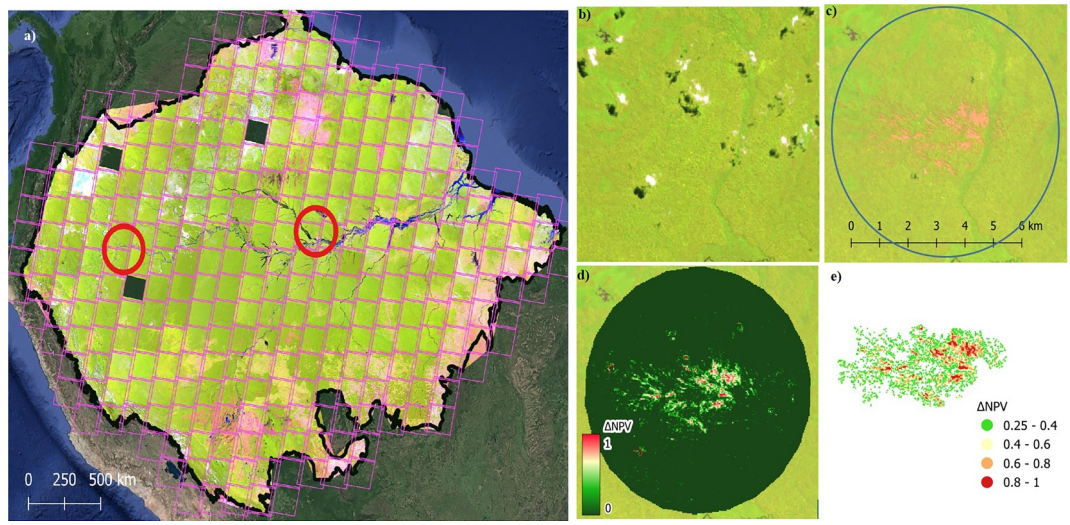

Figure 2. Study area and methods. (a) Example of an annual mosaic over the Amazon biogeographic limits (black line) comprising each Landsat 5/8 tile (purple lines) from which the images with minimum cloud cover were selected for the target years (e.g., in 2000, the year shown). Empty squares are scenes where no image with cloud cover <50% was available (these were omitted from further analysis in that year); and areas where field data on windthrow tree-mortality were collected (red circles) and combined with Landsat 5 TM (1985–2010) and Landsat 8 OLI (2015 and 2020). (b) Pre-disturbance image for an area where a 2020 windthrow was identified. (c) Post-disturbance image as example of a target windthrow, with the designation of buffer of 4 km of radius (blue circle) used to reduce false-positive detections and subsequent computational efforts. (d) Changes in non-photosynthetic vegetation (ΔNPV). (e) Spatial aggregation of events used to reduce scattering effects around windthrows and respective ΔNPV values.

and fractions of these endmembers, called abundances. The linear unmixing model has received considerable attention since it generally consists of an acceptable first-order approximation of the physical processes involved in most scenes of interest (Garg, 2020). Two distinct endmembers associated with windthrows were quantified: green photosynthetic vegetation (PV) and non-photosynthetic vegetation (NPV) (attributable to dead or broken tree stems). After observing no differences in windthrow detection using different NPV endmembers (see Figure S2 in Supporting Information S1), we used the average of a set of endmembers for the different Landsat sensors to characterize windthrows across the entire basin.

We used SMA to quantify the fraction of PV and NPV for each pixel. The fractions of NPV were then normalized as $\mathrm{NNPV} = \frac{\mathrm{NPV}}{(\mathrm{PV}+\mathrm{NPV})}$ (Adams & Gillespie, 2006). Normalization removes artifacts associated with seasonal or orbital differences in the background PV signals when comparing the cloud-free images (before and after the windthrow) acquired in different months. We computed ΔNPV by subtracting $\mathrm{NNPV}_{\text{target year}} - \mathrm{NNPV}_{\text{target year}-1}$. The severity of windthrow tree-mortality was scaled to range from 0 (old-growth forest) to 1 (highly disturbed, >90% mortality) (Figure 2d). This approach has been employed in previous studies that combined field and remote sensing data in the central (Brazilian) (Emmert et al., 2023; Marra et al., 2014, 2018; Negrón-Juárez et al., 2011, 2018) and western (Peruvian) Amazon (Rifai et al., 2016; Urquiza Muñoz et al., 2021) (Figure 2a, locations identified with red circles).

To minimize false positive windthrow detections we applied a 100 m buffer for minimizing the error caused by the edges of masked cloud-covered areas. Further, we visually identified the characteristic shape of windthrows as either diverging from a central area with corridors separated by undisturbed forest or exhibiting radial or fan-shaped patterns (Araujo et al., 2017; Nelson et al., 1994) (Figure 2c). Confirmed windthrows were manually labeled and enclosed in a buffer circle with 4 km radius (Figure 2c, blue circle). These circles were used to reduce the computational effort when calculating metrics such as area and severity of single windthrows. When an additional windthrow occurring in the same year was identified within the same radius such that the circles overlapped, we counted this as a single windthrow event and reported the summed area over the various windthrow "patches." To reduce the false positives around affected areas–usually attributable to local variations in tree phenology, deciduousness or fog–we focused our analysis on pixels with $\Delta\mathrm{NPV} \geq 0.25$ (Y. Feng, Negrón-Juárez, Chiang, & Chambers, 2023; Feng, Negrón-Juárez, Romps, & Chambers, 2023). Then, windthrows were clustered

using a morphological reducer tool available in GEE (focal mode; radius = 1, kernel type "square," units = "pixels," iterations = 1) (Figure 2d). Morphological operations minimize interference and enhance object edge details, separates overlapping objects in low-resolution multispectral images, extracting valuable information (Dharani & Sreenivasulu, 2021). Our estimates of windthrow area are thus deliberately conservative and limited to the core area to meet the requirement that pixels with $\Delta NPV \geq 0.25$ be connected (e.g., compare Figures 2d and 2e).

Post-processing steps included a detailed verification and classification of detected windthrows to reflect levels of uncertainty around our detection approach. To do this, we compared the point cloud distribution with the visual outline of drawn polygons and respective windthrows identified automatically in the raw imagery data (Figure S3 in Supporting Information S1). Class-1 windthrows had full agreement between the point cloud distribution and the identified disturbed patch (Figure S3a in Supporting Information S1). These provided the most reliable and conservative estimates of windthrow-affected area. Class-2 windthrows did not match the actual disturbed patch, which led to underestimation of the true windthrow area (Figure S3b in Supporting Information S1). This occurred when clouds covered part of the target windthrow area in the previous year. Class-3 windthrows occurred when the point cloud distribution exceeded the margins of the disturbed patch, leading to overestimation of the disturbed area (Figure S3c in Supporting Information S1). Class-4 encompasses all events that cannot be compared on an annual basis, as the target year provided the only available data–that is, cases where the ΔNPV and the event size cannot be estimated. We report the number of windthrow events for each year based on all detected windthrows, but constrained our estimates of size and severity distribution only to Class 1 events for which we have highest confidence.

2.2. Spatial Distribution and Clustering of Windthrows

To determine whether there were "hotspots," or areas where windthrows occur with greater frequency, we applied a clustering analysis by imposing a 20 km × 20 km grid over the defined area of the Amazon Basin. We estimated the centroid for each event by averaging the coordinates of the pixels within the defined disturbed points for all windthrow events and years. Using the centroids, the spatial density of windthrows was calculated at a 20 km resolution by kernel density estimation using an Epanechnikov kernel with a bandwidth of 200 km (function *kde* in package *SpatialKDE* in R) (Caha, 2023). The spatial density was calculated for individual years. The latitude and longitude density were estimated by the spatial distribution of centroids and plotted in a map using the function ggMarginal in the package ggExtra in R (Attali & Baker, 2023).

2.3. Estimation of Windthrow Area and Severity (Windthrow Inventory Database, WInD)

For Class-1 windthrows, the area directly affected was determined by identifying pixels with $\Delta NPV \geq 0.25$ within each polygon that shared at least one edge with another pixel having $\Delta NPV \geq 0.25$. To accomplish this, we extracted the centroid of each polygon and spatially aggregated all contiguous pixels. These pixels were also used to extract the spatial distribution of windthrow severity (Figure 2e). To obtain conservative estimates, we limited our analysis to windthrows with a minimum area of 30 ha (i.e., ≥333 Landsat pixels) and in which the fan shape typical of large windthrows could be observed. As a demonstration of sensitivity to our constraint that contiguous pixels delimit the core of the windthrow, we tested an alternative method that created a polygon by connecting single pixels that outlined the core area using the Concave Hull algorithm (parameter concavity = 3) in the concaveman package (Gombin et al., 2020) (see Figure 3).

As Class-1 windthrows represented more than half of the detected events (see Results), and were those for which we have high confidence in area estimates, we used them to calculate the size and severity distributions of events. In order to identify optimal models for characterizing the size distribution of windthrows, we employed the Akaike information criterion (AIC) methodology. The AIC is a mathematical method for evaluating how well a model fits the data from which it was generated. In statistics, AIC is used to compare different possible models and determine which one has the best fit to the data (Stoica & Selen, 2004). The AIC is accessible within the univariate ML 1.1.2 package in R (Moss, 2019). Given that all data are positive, we only evaluated support densities on the positive half-track.

To provide an estimate of the total Amazon basin area affected by windthrows in a given year, we adopted a yearly average area determined for Class-1 events and multiplied this by the sum of the number of other events (i.e., sum of Class 2, 3, and 4 events) in the respective year.

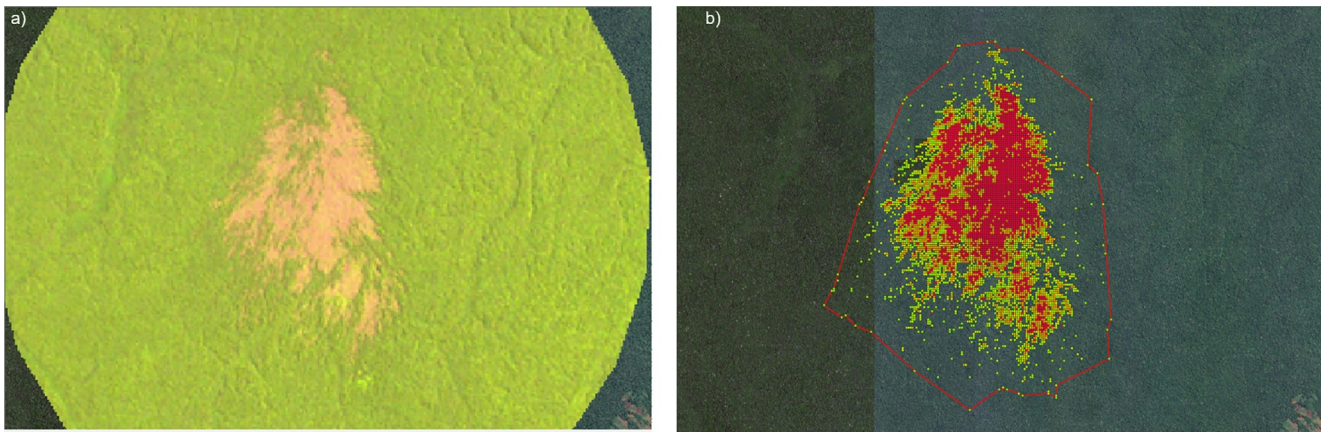

Figure 3. Direct and indirect affected area. (a) Verified windthrow. Note that at the bottom right corner of the image (outside the circle) there is an area that is disturbed but not classified as a windthrow due to its rectangular boundaries that identify it as land-use related disturbance. (b) Our detection Class 1 points were distributed within the directly affected area, defined by requiring at least one adjacent disturbed pixel, which totaled approximately 604 ha. The indirectly affected area, as indicated by the red polygon, was calculated using the Concave Hull algorithm (parameter concavity = 3) in the concaveman package, resulting in a total of approximately 1,630 ha.

All detected windthrows were organized, structured, and stored in our *Windthrow Inventory Database*, Version 1.0 (WInD V.1) (Urquiza-Muñoz et al., 2024). The WInD V.1 includes a complete catalog of windthrows detected in the 33 years we studied, and a detailed summary of their attributes (e.g., area, windthrow severity and the spatial distribution of pixels) (see Figure S4 in Supporting Information S1). WInD V.1 is available as an open-access resource (https://doi.org/10.5281/zenodo.11168104).

2.4. Analysis of Climate Indicator Data

Large windthrows provide a record of the impact of strong convective storms that cause downdrafts with the energy to damage areas ≥30 ha. Our results thus provide a history that could be used to improve modeling and prediction of such storms and their ecosystem relevance. While atmospheric modeling for detailed attribution of the causes of trends and interannual variability are beyond the scope of this study, we compared commonly used climate indicators with our temporal and spatial records. Specifically, we used data on the Oceanic Niño Index (ONI), the Atlantic Meridional Oscillation (AMO) and the CAPE to assess their degree of correlation with interannual variability or temporal trends in windthrow occurrence. The El Niño Southern Oscillation (ENSO) has been identified as a main driver of interannual climate extremes in Amazonia (Cai et al., 2020). ONI data was downloaded from the NOAA Weather Service Climate Prediction Center (https://origin.cpc.ncep.noaa.gov/products/analysis_monitoring/ensostuff/ONI_v5.php), where they are reported as the 3-month running mean of sea surface temperature anomalies in the Niño 3.4 region (5°N–5°S, 120°–170°W). ONI values >0.5 are considered indicative of El Niño (>1.0 indicates strong El Niño), while values <−0.5 indicate La Niña conditions (<−1.0 strong La Niña) (Bamston et al., 1997; Huang et al., 2017). We also accessed data on the detrended Atlantic Multidecadal Oscillation (AMO) index from the NOAA Physical Sciences Laboratory (https://psl.noaa.gov/data/correlation/amon.us.data) to compare with temporal trends in the windthrow data.

Previous work demonstrated that regions of dense windthrows (summed from 1990 to 2019) tend to be the regions where mean afternoon CAPE is large (Y. Feng, Negrón-Juárez, Chiang, & Chambers, 2023; Feng, Negrón-Juárez, Romps, & Chambers, 2023). Following the methods outlined in (Feng, Negrón-Juárez, Chiang, & Chambers, 2023; Feng, Negrón-Juárez, Romps, & Chambers, 2023), we obtained data on CAPE from ERA 5 hourly reanalysis data available at: https://cds.climate.copernicus.eu/cdsapp#!/dataset/reanalysis-era5-single-levels?tab=form.

Mean and extreme (upper 95th percentile) CAPE values were calculated from data limited to time periods when convective storms mostly occur: the local afternoon 13:00–19:00 (UTC 17:00–23:00) from August to November (e.g., August-November in 2010 to compare with windthrows reported as occurring in 2010).

3. Results

3.1. Windthrow Detection and Mapping

We analyzed 9,082 Landsat scenes (6,943 scenes of L5 TM and 2,139 scenes of L8 OLI) with cloud cover <50% (see Table 1 and Figure S2 in Supporting Information S1 for details of scene distribution). In total, we identified 3,179 disturbance patches classified as windthrows ≥30 ha (Table 1). The years 2012 and 2013 were excluded from the analysis because these were transition years between Landsat sensors, and this would affect our estimation of ΔNPV. We also excluded the year 2002 due to a large number of scenes with >50% cloud cover. The number of scenes analyzed varied from year to year (Table 1), averaging 267 scenes for the years with Landsat 5. These increased to an average of 298.7 scenes for the years after the switch to Landsat 8 in 2014, that is, the number of scenes increased by ∼10%. To correct for this effect on temporal trends in our results, we reduced the number of events detected after 2014 by 267/298 and included this in our analysis (corrected values are identified with an asterisk in Table 1; this reduced the number of total events to 3081 for analysis of temporal trends). As cloud-free scenes are concentrated in the eastern and southern Amazon in most years (Figure S5 in Supporting Information S1), it is likely that our approach is underreporting windthrows in areas with typically more clouds (western and northern Amazon) during the Landsat 5 record.

Of the 3,179 events identified, 1,819 (57.2%) were classified as Class-1 (i.e., events with cloud-free prior year images for which we can confidently estimate total area and severity [ΔNPV] distribution), 581 (18.3%) as Class-2 (i.e., bias toward underestimated area), 278 (8.7%) as Class-3 (i.e., bias toward overestimated area), and 501 (15.8%) as Class-4 (i.e., no prior year cloud-free image for ΔNPV estimation). Class-1 accounts for more than 50% of all observations in every year except for 1985, 2001, and 2015, when they were 49%, 48%, and 46%, of events, respectively.

Classes 1 and 3 are well distributed throughout the Amazon basin, however, Classes 2 and 4 (both of which involve clouds obscuring the prior year image) tended to occur more in the northwest Amazon (see Figure S5 in Supporting Information S1) which is the area of the Amazon with the highest precipitation. Thus, the potential for errors in estimating total windthrow area are smallest in the parts of the basin with least cloud cover (south and east) and greatest in those with consistently higher cloud cover (north and west). A comparison of the number of windthrows divided by the number of scenes analyzed indicates limited biases, even when more images were available after 2014 (see Figure S6 in Supporting Information S1).

The map of windthrows we have produced generally has limited overlap with products of forest loss/gain produced using other criteria. In cases where ΔNPV values indicate severe forest damage (ΔNPV >0.8), these can be (and in some cases were) classified as forest loss (Hansen et al., 2013). Thus, distinguishing windthrows from other types of forest disturbance such as deforestation still requires manual inspection (as performed in this study; see also Figure 2 for an example) of the spectral and geometric characteristics of disturbed patches.

3.2. Spatial Distribution of Windthrow Events

We detected windthrows throughout almost the entire Amazon basin (see Figure S5 in Supporting Information S1), although in some regions they are very rare. We defined windthrow density as the number of events occurring in cells within a 20 km × 20 km grid imposed across the study area (see Section 2.2). Our data indicate a distinct clustering characterized by significantly greater density of windthrows (density ranging from 1 to 5 events/400 km^2 over the 33 years for which data are available, Figure 4) in the central and western Amazon. Areas of higher windthrow density (≥1 event over 33 years) cover approximately 14% of the Amazon basin (∼1,030,000 km^2), but account for ∼45% (1,448) of all detected windthrows. Areas with ≥2 events over 33 years represent ∼3% of the Amazon Basin and are ∼35% (1,118) of all detected windthrows.

Across all years, windthrows occurred most frequently between the equator and 5° S (Figure 4b). The areas with highest windthrow density oscillate over time, particularly longitudinally between the central and western Amazon (Figure 4a), as reflected in the fluctuation of intensity and location of windthrow density aggregated by 5-year intervals (Figure 4a).

Table 1
Summary of Detected Windthrows

Year	Scenes	ACC	Events	Ratio events/ scenes	Class1	Class2	Class3	Class4	Avg size	Median size	Max size	Affected by C1	Total estimated affected area
1985	227	8.2	78	0.34	29 (37%)	9 (12%)	8 (10%)	32 (41%)	103 ± 32	65 ± 20	351	2,995	8,042
1986	275	8.6	75	0.27	38 (51%)	6 (8%)	2 (3%)	29 (39%)	116 ± 58	72 ± 20	480	2,083	6,375
1987	260	7.2	45	0.17	35 (78%)	5 (11%)	2 (4%)	3 (7%)	105 ± 53	64 ± 17	618	2,617	3,667
1988	267	6.8	101	0.38	54 (53%)	25 (25%)	13 (13%)	9 (9%)	140 ± 40	93 ± 10	677	6,558	13,138
1989	264	6.6	58	0.22	42 (72%)	8 (14%)	1 (2%)	7 (12%)	80 ± 18	54 ± 10	249	2,568	3,848
1990	272	8.0	105	0.39	61 (58%)	5 (5%)	8 (8%)	31 (30%)	157 ± 51	85 ± 21	1,195	9,588	16,496
1991	278	5.6	41	0.15	29 (71%)	2 (5%)	9 (22%)	1 (2%)	127 ± 46	92 ± 35	417	2,928	4,452
1992	258	7.6	51	0.20	31 (61%)	9 (18%)	6 (12%)	5 (10%)	82 ± 19	64 ± 17	179	1,723	3,363
1993	258	7.6	52	0.20	28 (54%)	12 (23%)	6 (12%)	6 (12%)	178 ± 109	110 ± 55	1,029	3,387	7,659
1994	248	8.2	46	0.19	27 (59%)	11 (24%)	4 (9%)	4 (9%)	149 ± 135	72 ± 32	1,348	2,980	5,811
1995	254	6.3	123	0.48	70 (57%)	14 (11%)	17 (14%)	22 (18%)	180 ± 62	90 ± 21	1,878	12,601	22,141
1996	281	7.4	67	0.24	38 (57%)	14 (21%)	3 (4%)	12 (18%)	115 ± 36	85 ± 24	422	3,790	7,125
1997	288	7.4	71	0.25	49 (69%)	5 (7%)	11 (15%)	6 (8%)	155 ± 51	92 ± 18	681	6,188	9,598
1998	289	7.2	81	0.28	40 (49%)	21 (26%)	11 (14%)	9 (11%)	198 ± 77	126 ± 60	989	7,328	15,446
1999	286	7.4	125	0.44	74 (59%)	20 (16%)	22 (18%)	9 (7%)	176 ± 66	84 ± 12	1,608	11,087	20,063
2000	289	9.3	125	0.43	76 (61%)	16 (13%)	6 (5%)	27 (22%)	155 ± 37	102 ± 24	1,036	11,814	19,409
2001	259	3.9	72	0.28	35 (49%)	21 (29%)	8 (11%)	8 (11%)	102 ± 30	66 ± 14	412	3,365	7,139
2003	254	7.8	48	0.19	25 (52%)	7 (15%)	6 (12%)	10 (21%)	64 ± 21	53 ± 14	200	1,093	2,565
2004	268	7.2	35	0.13	20 (57%)	7 (20%)	4 (11%)	4 (11%)	93 ± 31	68 ± 20	211	1,396	2,791
2005	270	5.3	151	0.56	87 (58%)	19 (13%)	6 (4%)	39 (26%)	184 ± 42	131 ± 54	1,207	16,000	27,776
2006	271	6.3	56	0.21	30 (54%)	14 (25%)	11 (20%)	1 (2%)	141 ± 44	104 ± 33	478	3,654	7,320
2007	267	7.4	149	0.56	91 (61%)	26 (17%)	23 (15%)	9 (6%)	132 ± 31	86 ± 17	779	10,143	17,799
2008	271	4.9	56	0.21	35 (62%)	11 (20%)	3 (5%)	7 (12%)	153 ± 50	109 ± 42	413	3,671	6,884
2009	274	5.8	84	0.31	50 (60%)	23 (27%)	1 (1%)	10 (12%)	104 ± 47	63 ± 11	531	2,490	6,026
2010	248	7.2	186	0.75	105 (56%)	40 (22%)	27 (15%)	14 (8%)	254 ± 59	161 ± 53	1,860	26,682	47,256
2011	268	7.3	166	0.62	91 (55%)	50 (30%)	14 (8%)	11 (7%)	92 ± 25	74 ± 25	478	3,956	10,856
2014	267*	8.7	57*	0.21	39 (61%)	13 (20%)	0 (0%)	12 (19%)	133 ± 49	75 ± 18	617	4,244	7,569
2015	269*	6.5	163*	0.60	84 (46%)	26 (14%)	15 (8%)	57 (31%)	144 ± 30	87 ± 26	653	12,062	26,174
2016	264*	7.1	53*	0.20	42 (71%)	12 (20%)	4 (7%)	1 (2%)	120 ± 46	75 ± 13	853	4,557	6,597
2017	266*	6.5	137*	0.51	97 (63%)	37 (24%)	1 (1%)	18 (12%)	137 ± 102	63 ± 14	2,544	6,719	14,391
2018	269*	7.6	97*	0.36	78 (72%)	21 (19%)	4 (4%)	5 (5%)	94 ± 19	64 ± 9	341	5,182	8,002
2019	265*	8.4	91*	0.34	56 (55%)	33 (32%)	10 (10%)	3 (3%)	128 ± 49	62 ± 9	798	5,643	11,531
2020	269*	6.0	236*	0.88	133 (50%)	39 (15%)	12 (5%)	80 (30%)	150 ± 40	79 ± 8	1,803	19,999	39,649

Note. Columns: Year: studied year; Scenes: number of processed scenes; ACC: mean area of cloud cover across processed scenes, Events: number of detected windthrows ≥30 ha; Ratio events/scenes: number of events detected/number of scenes with <50% cloud cover, a measure of bias in years with high cloud cover. Windthrow classification: percentage of windthrows belonging to our classes of detection. Class 1 = greatest certainty in area estimate; Class 2–reduced certainty, likely underestimating actual area; Class 3 = reduced certainty, likely overestimate of actual area; Class 4 = Cases where the ΔNPV and the size cannot be estimated due to lack of scene from the previous year; Avg size: mean area (in ha) of all Class-1 windthrows in that year. Max size: maximum size (ha) of an individual windthrow detected in each year. Affected by C1: sum of the area values for Class 1. Total affected area–The estimated total area (in ha) affected is the sum of the area values for Class-1 events (Affected by C1) and the mean size determined from Class 1 events multiplied by the sum of Class-2, 3, and 4 events for that year.

3.3. Size and Severity Characteristics Based on Class-1 Windthrows

Class-1 windthrows (Figure S3a in Supporting Information S1), which account for 57% of the detected events, provide the most reliable estimates of the distribution of size (number of pixels classified as windthrow, i.e.

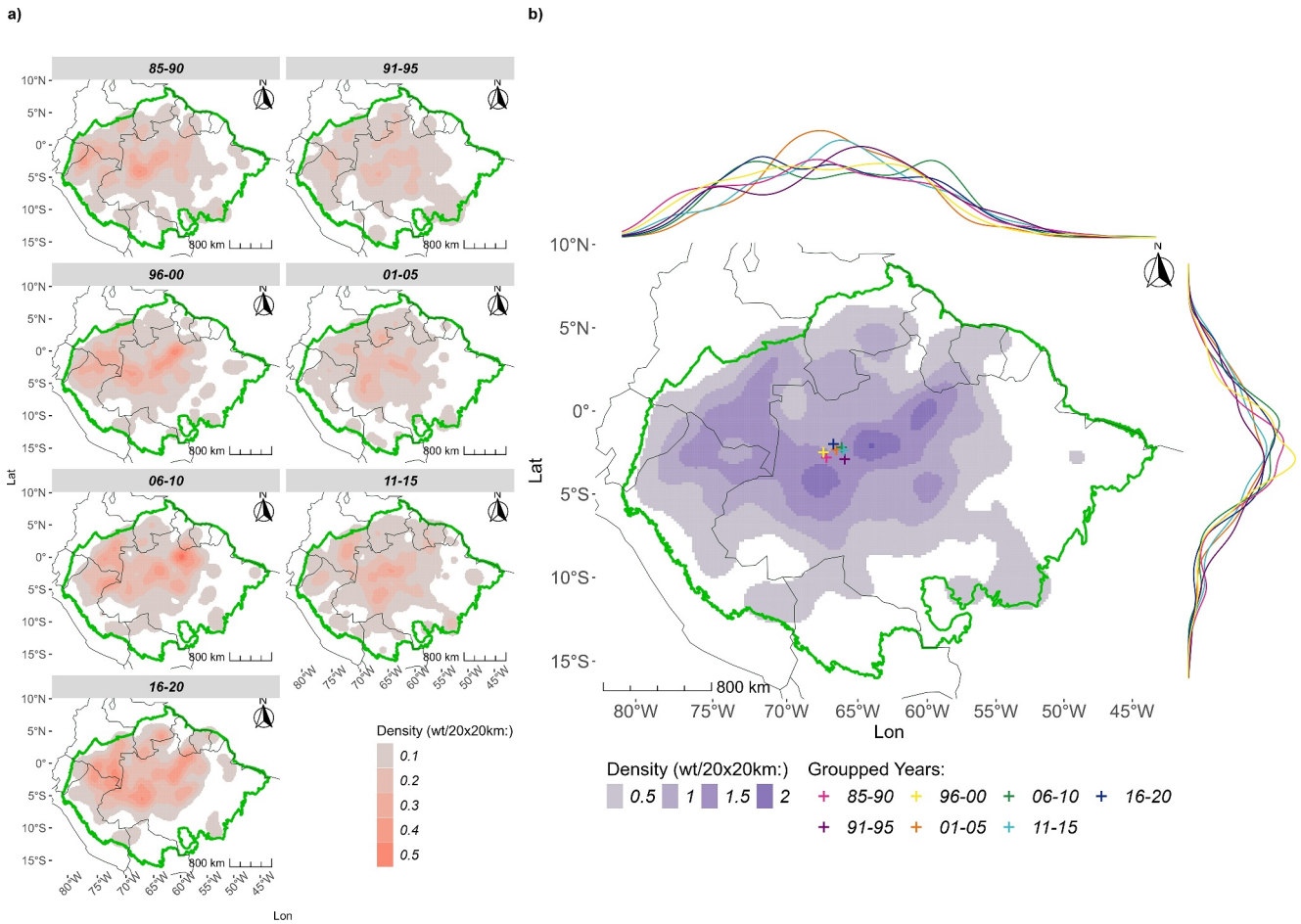

Figure 4. Spatial and temporal distribution of all detected Amazon windthrows ≥30 ha (Events in Table 1) for the period from 1985 to 2020. Density (color contour) is defined as the number of windthrows that occur in a 20 km × 20 km grid per year, (a) windthrow density aggregated over 5-year intervals. (b) Aggregated windthrow density over all 35 years. The Amazon basin area is delimited by the green boundary. Colored crosses (b) show the centroid locations of all windthrows detected in the grouped years. The colored density curves in the figure margins show the density distribution of windthrows across longitude and latitude for the aggregated 5-year intervals.

ΔNPV > 0.25) and severity (ΔNPV value for each pixel) for individual events (Table 1). Across the Amazon basin, the size distribution of Class-1 windthrows in any given year was highly skewed toward smaller events (Figures 5c and 5d). While the majority of windthrows had areas between 30 ha (our low end cutoff) and 200 ha, the maximum windthrow size observed was ~2,543 ha (year: 2017, ~260 km north of Porto Velho, Brazil, Lat:−6.8207035, Long:−62.3252312), and the number of events greater than the upper quartile occurred mostly in 2 years, 1995 (11 large events), and 2020 (16 large events). The disturbed area attributable to a few large events (here defined as windthrows >500 ha) can make up a relatively large fraction of the total area disturbed in a given year (Figure 5b) and is responsible for much of the interannual variation in the mean size of windthrows in any given year (Table 1). The same patterns were also observed in hotspot areas (Figure S7 in Supporting Information S1).

The median size overall years for Class-1 windthrows was 84 ± 5 ha. The mean was 147 ± 13 ha (99% CI), ranging from a minimum of 64 ha in 2003 to a maximum of 252 ha in 2010 (Table 1). However, windthrows occurring in hotspot areas (density ≥1; Figure 4) averaged nearly twice the size of this basin-wide average ~284 ± 57 ha (99% CI). Post-hoc pairwise comparisons using *t*-tests with pooled SD (p-adjusted using the false discovery rate method) indicated no significant ($p > 0.05$) trends in the mean size of Class-1 windthrows over time. Only the year 2010 had significantly ($p < 0.05$) greater (254 ha) mean area compared to other years (Table S1 in Supporting Information S1).

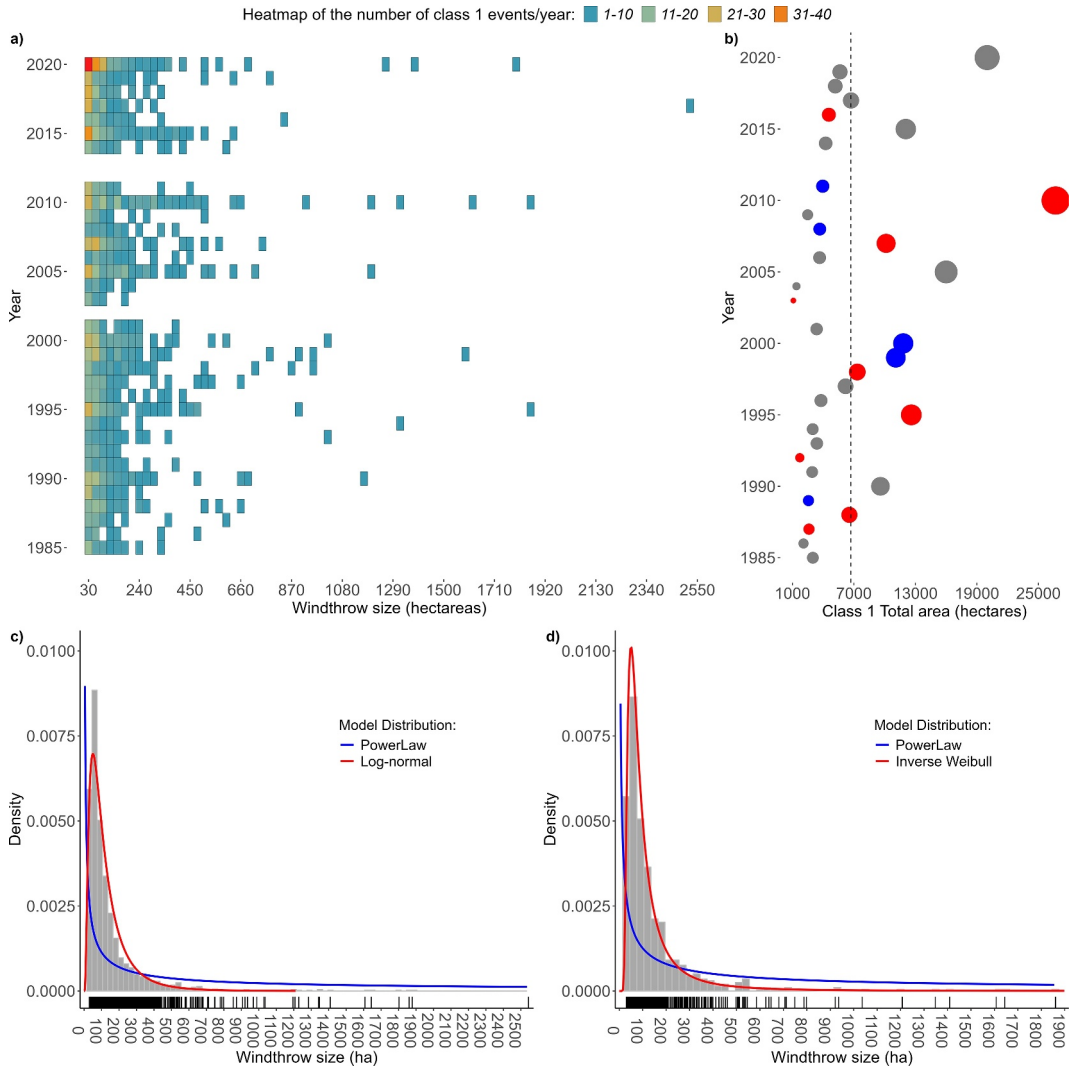

Figure 5. The optimal models for large windthrow size distribution. (a) Heatmap of event size by year. The heatmap depicts the number of years that a given windthrow size has occurred on the *y*-axis, with the size represented on the *x*-axis. The color intensity in each cell represents the frequency of windthrows within that specific size category and year. (b) Temporal variability of total disturbed areas by year, the dashed line shows the mean total affected area (~6,700 ha) across all years, color represents the strong El Nino (red), La Nina (blue) and neutral (gray) years. In total 221,090 ha of forest were disturbed in Class 1 events over the 33 years with observations between 1985 and 2020. (c) Distribution of the frequency (histogram bin = 30 ha) of events in size classes of 100 ha intervals (i.e., 0–100 ha, 100–200 ha, etc.) across all years for the Amazon basin compared to two models; the "Log-normal distribution maximum likelihood" model with an Akaike information criterion (AIC) far below the power law distribution or other candidate models (See Table S2 in Supporting Information S1). (d) Frequency-area distribution (histogram bin = 30 ha) for hotspot areas, where the "Inverse Weibull distribution maximum likelihood" model stands out with an AIC far below the power law distribution or other candidate models.

Windthrow severity was assumed to scale with ΔNPV values, ranging from minimal disturbance (below our lower cutoff of 0.25) to moderate (0.25–0.5) and severe (>0.5) damage, with 1.0 representing complete loss of photosynthetic vegetation (i.e., 100% of windthrow tree mortality) (Emmert et al., 2023; Marra et al., 2018; Urquiza Muñoz et al., 2021). The cumulative distribution of windthrow severity, that is, the total number of pixels identified in Class-1 windthrows with a given severity in each year had a consistent unimodal distribution across the analyzed years (Figures S8a and S8b in Supporting Information S1), and did not demonstrate any apparent trend over time. Notably, 2010 and 2020 were marked by severe windthrow events and had the highest number of pixels with ΔNPV values ≥0.5. Because we rely on only two locations for which our end members

were field-calibrated (Manaus and Iquitos) and can thus not address potential regional differences, we will not discuss patterns or trends in severity in this study.

3.4. Total Projected Area Damaged by Windthrows

Our method allowed us to accurately detect the number of ≥30 ha windthrow events. For 57% of events classified as Class 1, we could confidently determine their individual area. To provide an estimate of the total area affected by all detected windthrows each year, we included the Class-1 detected area and added the number of non-Class-1 events (i.e. summing Class 2, 3, and 4) multiplied by the mean area as determined from the Class-1 events that year. Obviously, we can have limited confidence in this extrapolation. Still, we are most confident for estimates covering the central and eastern Amazon, where most of detected windthrows fall in Class-1 (see Figure S5 in Supporting Information S1).

Using this method and summing over the 33 years of record for which we could identify windthrows between 1985 and 2020, we estimated a total moderate-to-severely disturbed area of 423,000 ha, or roughly 0.06% of the ~7,000,000 km^2 area of the Amazon basin. This implies a disturbance rate for windthrows ≥30 ha of 0.0018% per year, or average return interval of ~55,000 years. However, our spatial analysis shows that windthrows are concentrated in hotspot areas, such that only 14% of the basin had ≥1 windthrow over 33 years. Within those regions, windthrows had larger mean areas (~270 ha) compared to the basin-wide averages (~150 ha). We estimate the total area disturbed ~186,000 ha (0.18% of the hotspot area in 33 years), which implies a disturbance rate of 0.0054% yr^{-1}, or a return interval of ~18,000 years. These estimates are based on severe disturbance within large and potentially less-frequent events without consideration of the forest corridors that can be affected by neighboring damage in subsequent years (see Figure 2d), or less impacted areas on the edge of contiguous moderate to severe damage (e.g., Figure 3). The Concave Hull algorithm shows an increase of the estimated area affected of 2.3 ± 0.08 (mean ± 99% CI, number of windthrows analyzed = 519). See for example, the windthrow in Figure 3, where the affected area increases from 706 to 1,630 ha (i.e., 2.3 times more affected area). Calculating the actual area impacted by a windthrow including areas outside the major disturbed patch requires care and field confirmation. For Class-1 events we found that the area of impact can be up to three times greater than the area we reported depending on how the boundary is drawn (e.g., Figure 3).

Large-scale windthrows such as those we identified here can thus be considered rare events over much of the Amazon basin. However, within hotspot areas, we have detected 20 km × 20 km areas with 2–5 windthrow events ≥30 ha in size over the 33 years of record. These represent in total around 3% of the area of the basin, but about a third of the total events. In these areas, we estimate that from 1.35% to 3.4% of the area experienced severe wind damage/mortality in 33 years, or recurrence intervals of ~1,000–2,500 years (see Figure 6 for examples). As noted above, our area estimates are conservative and represent just the core area experiencing moderate to severe damage. In fact, we expect the actual area affected to be larger, and thus recurrence intervals in these regions could potentially be of the order of three lifetimes (hundreds of years; Vieira et al., 2005) (Figures 2d and 3).

The size distribution of Class 1 windthrows from 1985 to 2020 are illustrated with a heatmap (Figure 5a). Prior to the 1990s, the majority of windthrows had sizes of <750 ha Figure 5a also shows that smaller size categories (between 30 and 250 ha) have become more common in recent years than in the past, and that this has been accompanied by an increase in the occurrence of large events (between 750 and 2000 ha). These large-scale events contribute substantially to the total area affected on an annual basis (Figure 5b; Table 1).

Given the large number of windthrows we have identified, we tested the hypothesis that their size -frequency distribution follows a power law (e.g., as suggested in Chambers et al., 2009, 2013; although Espírito-Santo et al., 2014 note breaks in slope of power law distributions). According to our AIC analysis (See Table S2 in Supporting Information S1), applied only to Class-1 windthrows, size-frequency distributions did not fit the power law distribution. More optimal models for the size distribution of windthrows ≥30 ha in the Amazon basin were the Log-normal (df = 2, AIC = 20783.78) and Log-gamma (df = 2, AIC = 20837.49) models (see Figure 5c). Like the Log-normal and Log-gamma distributions, the Weibull distribution can also be used to model the asymmetric windthrow size distribution. In hotspot areas, the inverse Weibull (df = 2, AIC = 7533.932) and inverse gamma (df = 2, AIC = 7548.182) were the optimal models (see Figure 5d).

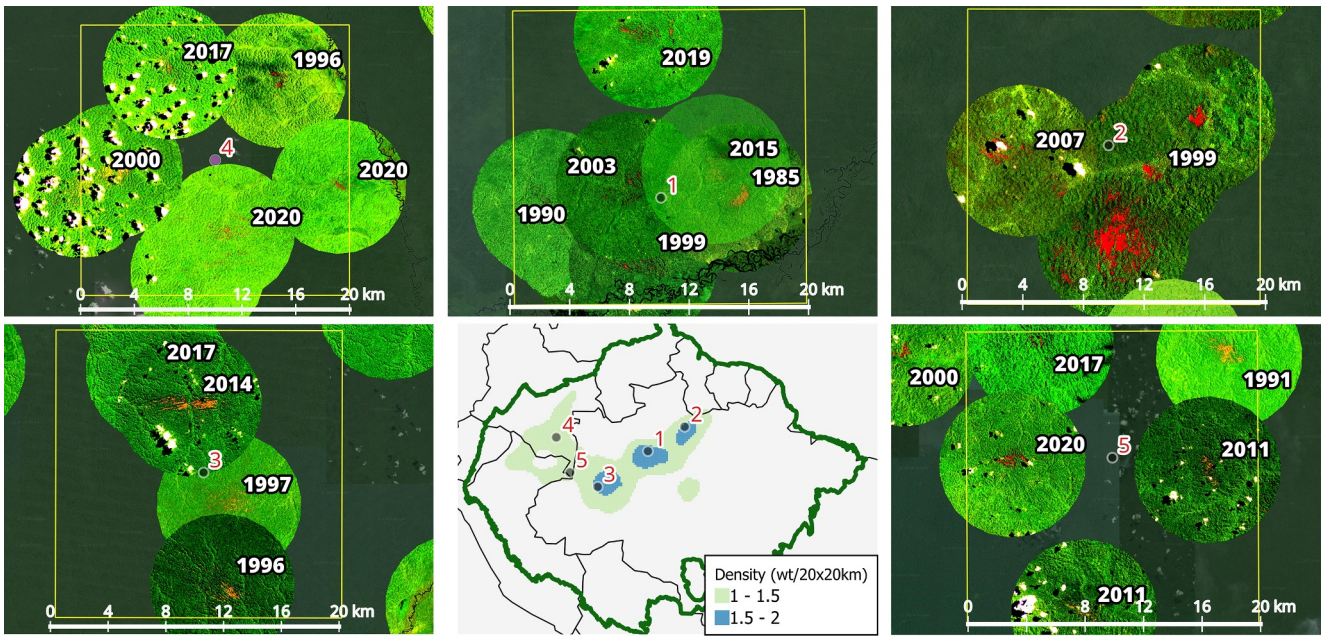

Figure 6. Examples of areas within "hotspots" where multiple windthrows ≥30 ha occurred in a 20 km × 20 km area over the 33-year period. The white numbers represent the year of occurrence of windthrows. Black numbers and dots represent the location. The yellow lines show the extent of the 20 km × 20 km grid.

3.5. Temporal Trends in Windthrows

Fitted linear regressions (Figure 7a) show that both the number and the estimated total area of windthrows ≥30 ha increased significantly from 1985 (50 events) to 2020 (205 events). The total number of events was assessed with high confidence, whereas the confidence is lower for estimates of total area as it was based on Class-1 areas (high confidence) and the areas for Class-2, 3, and 4 (relatively lower confidence). The positive slopes of both fitted models suggest that the number of windthrows and associated area increased at rates averaging 3 windthrows yr^{-1} and ~340 ha yr^{-1} over the last 35 years.

Figures 5 and 7 also demonstrate large interannual variability both in the number and estimated area affected by windthrows, with variability increasing especially in the last half of the record. To assess potential relationships between interannual variability and trends in windthrows we compared them with common indices related to tropical climate variability (ENSO/La Niña) and Atlantic Multidecadal Oscillation (AMO), as well as to CAPE. In seeking attribution using temporal comparisons, we need to acknowledge that the actual climatic (windthrow-causing) storm event could have occurred in the calendar year before we reported it. Because most of the cloud-free Landsat images occur in dry-season months (that tend to be in June through October), a windthrow detected and reported in a given year (e.g., 2006), could potentially have been caused by an event that occurred in the second half of the previous one (e.g., 2005). In the case of CAPE, the maximum values in a given year tend to be in the months of August-November, and we compared the same year in which the windthrow was reported (see Methods).

El Niño and La Niña years are associated with anomalous temperatures in the eastern Pacific ocean and drive much of the interannual variation in Amazon rainfall, with recent record droughts occurring mostly during El Niño years (1987, 1998, 2010, 2016, but not 2005) and years with large flooding (1989, 1999, 2009, 2012, 2022) during La Niña years (Marengo et al., 2018). As also found by Negrón-Juárez et al., 2017, we found no significant relationship between the ONI value and the number or area of windthrow (Figure S9 in Supporting Information S1). For example, although 2010 was an El Niño year with a relatively high number of windthrows, the stronger ENSO years of 1998 and 2016 were not marked by large numbers of windthrows. There has been no overall temporal trend in ONI over the past three decades (Figure S9 in Supporting Information S1), although windthrows have increased. The Atlantic Multidecadal Oscillation (AMO) is related to shifts in sea surface temperatures in the north Atlantic Ocean, where warmer temperatures (positive AMO phase) have also been related to increased Amazon droughts (Espinoza et al., 2019; Yoon & Zeng, 2010). During the period we studied here, the AMO index

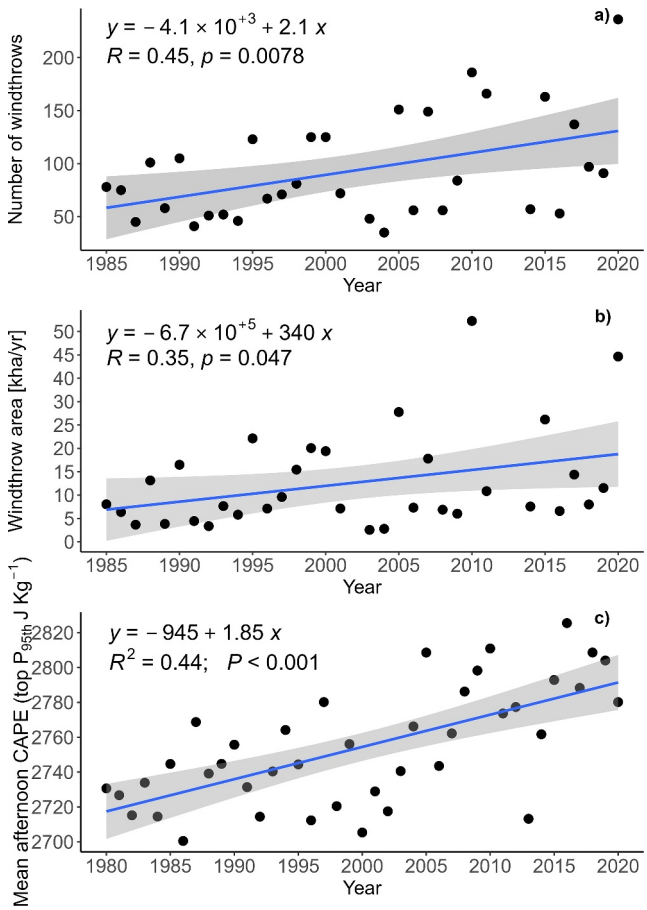

Figure 7. Trends. (a) Corrected number of windthrows ≥30 ha per year between 1985 and 2020. Linear regression models (with 95% confidence interval) indicate a mean increase at rates of ~2 windthrows/year or 340 ha/year. (b) Total summed windthrow area. Total summed areas could be up to 10% less for each year after 2014 (related to change in cloud cover with Landsat sensor; see text) but also show an increasing trend. (c) Mean extreme afternoon Convective Available Potential Energy (95th percentile from ERA5) for all years.

(detrended; https://psl.noaa.gov/data/timeseries/AMO/) increased from a cold (−0.2) to a warm phase (high of 0.9 in 2017). However, as with ONI, we did not see evidence for AMO linking to interannual variability in windthrow numbers or area.

The top 95th percentile of afternoon CAPE values averaged over the entire Amazon basin indicated a small but consistent increase in absolute values from 1985 to 2020 (Figure 7b), even though the mean CAPE values have declined over the same period (Riemann-Campe et al., 2009). The spatial distribution of the 95th percentile afternoon CAPE overlaps with observed windthrow density (Figure S10 in Supporting Information S1), indicating a larger-than-average increase of extreme CAPE values in the western Amazon, where the number and area of windthrows increased the most over the same time period (Figure 7c).

4. Discussion

The observed increase in the number of windthrows and the area they have affected between 1985 and 2020 across the Amazon Basin provides important information for assessing possible changes in convective storms and their impact on forests. Windthrows provide evidence of where and approximately when strong downdrafts occurred in the past. This information is especially important for a region such as the Amazon Basin, where long-term observations of forest dynamics and atmospheric conditions are sparse. As large windthrows trigger ecological and biogeochemical changes, our data indicate which regions in the Amazon are most likely to be impacted by windthrow damage.

4.1. What Could Explain the Observed Increase in Windthrow Number and Area Since 1985?

Our results document a nearly fourfold increase in the number and accumulated area of windthrows ≥30 ha from 1985 to 2020. One plausible explanation for this increase is related to the intensification of the Amazon's hydrological cycle in the last two decades (Gloor et al., 2013), and to changes in larger-scale circulation that reflect trends in the AMO and ocean surface warming (Barichivich et al., 2018). Such changes include the enhancement of deep convective clouds and intense rainfall, and positive anomalies of terrestrial water storage over the northern Amazon during the 21st century (Espinoza et al., 2022), as well as increases in extreme flooding events (Barichivich et al., 2018). With climatic warming, atmospheric conditions favorable for the formation of extreme storms over tropical regions are expected to increase (Diffenbaugh et al., 2013; Seeley & Romps, 2015; Singh et al., 2017), which could lead to a continued increase in windthrows (Y. Feng, Negrón-Juárez, Chiang, & Chambers, 2023; Feng, Negrón-Juárez, Romps, & Chambers, 2023), with a potential decrease in the atmospheric conditions producing weak and moderate storms (Rasmussen et al., 2020).

Although responsible for a large fraction of annual precipitation as well as severe weather, convective storms remain poorly understood. Our results add support from the Amazon region to evidence from radiosonde data for a global increase in unstable atmospheric conditions that can lead to extreme storms over the past 40 years (Chen & Dai, 2023). Characteristics of past windthrows (e.g., area, shape, damage distribution) could be used to infer properties of storms, though the degree of observed damage depends both on atmospheric conditions producing the downdraft and the vulnerability of the impacted forest to wind damage (Peterson et al., 2019; G. H. P. M. Ribeiro et al., 2016; Silvério et al., 2019). Over the past 35 years, the characteristics of intact Amazon forests are unlikely to have changed, and we did not see shifts in the windthrow size or severity distributions over time. Therefore, we attribute the increase in large-scale windthrows primarily to changes in atmospheric conditions.

Changes in the frequency of strong convective storms since 1985 could reflect variation in the local atmospheric environment in which convective storms develop (e.g., static instability), or even other conditions that could affect the speed and duration of downdrafts (Garstang et al., 1998). While a previous study noted the spatial overlap between high values of CAPE with the "hotspot" regions where most windthrows occur in the Amazon (Y. Feng, Negrón-Juárez, Chiang, & Chambers, 2023; Feng, Negrón-Juárez, Romps, & Chambers, 2023), over the period 1985–2020 where we observed a large increase in windthrow occurrence, mean afternoon CAPE values declined over the Amazon basin (Riemann-Campe et al., 2009). Here, we demonstrated an increase in the mean top 95th percentile of afternoon CAPE values (increasing from ∼2,700 to 2,820 J kg^{-1}) in the Amazon region over the last 35 years (Figure 7c) that also had spatial overlap with the density of windthrows (Figure S10 in Supporting Information S1). Besides CAPE other variables can be used to predict damaging convective storms. For example, the study by Windmiller et al. (2023) found that the best predictors for downdraft mass flux and velocity were updraft properties that determine the rain amount and rate, and the environmental lapse rate. Observational and modeling studies of Derechos (strong convective storms in the central United States) suggest that the frequency of downdrafts is expected to increase with climate change (Prein, 2023), and that downdraft CAPE, a better predictor of strong near surface winds, should be explored in further analysis.

Although reflecting a global multidecadal trend of increased atmospheric instability that contributes to weather extremes (Chen & Dai, 2023), we are unable here to pinpoint a specific cause for increased windstorms. In addition to changes in atmospheric dynamics associated with detectable warming during this period (Marengo, 2004), another atmospheric change over the past 35 years in the Amazon is the amount of biomass burning aerosol, which has direct radiative effects and an impact on the number, chemistry and size of cloud condensation nuclei (Artaxo et al., 2013). Further, we did not find obvious explanations for the large interannual variations in windthrow occurrence using climate indices like ENSO that are generally tied to precipitation variability.

One value of our study is to provide evidence of past damage from large-scale convective storms for benchmarking cloud-resolving climate models. Further examination of specific windthrows in our database can narrow the timing of their occurrence, often to within a few weeks. This could be important for detailing the meteorological conditions associated with a specific event (Mendonça et al., 2023; Negrón-Juárez et al., 2015). Recent developments in cloud- (Satoh et al., 2019) and storm-resolving (storm-resolving models), and convection-permitting (Z. Feng et al., 2023) models, especially in the Amazon region (Rehbein & Ambrizzi, 2023; Tai et al., 2021), could be combined with basin-wide information on characteristics like forest structure available from field and LiDAR data. Long-term observations linking the temporal and spatial distribution of extreme wind and rain with local meteorological conditions and windthrow occurrence will also contribute to better addressing the dynamics and seasonality of these mechanisms of disturbance across topographic gradients.

4.2. How Important Are Large Windthrows for Amazon Forest Composition and Structure?

The pattern and severity of forest damage for a given windthrow are related to downdraft velocity and geometry, but also to the resistance of forest to wind (Fujita, 1990; Peterson et al., 2019; G. H. P. M. Ribeiro et al., 2016). Important factors include stand characteristics (tree height-to-diameter-ratio and tree density), the mechanical stability of occurring species (slenderness, crown size, root anchoring, soil depth and properties, and connections between trees and lianas) and interactions of downdraft winds with local topography. The large-scale windthrows reported here (≥30 ha) promote changes in environmental conditions that trigger secondary forest succession, with different species adapted to the rapidly changing levels of light, moisture, and nutrient availability in newly formed gaps. As a result, windthrows can promote biodiversity (Alencar et al., 2022; Marra et al., 2014), shape forest structure and biomass (Marra et al., 2018; Rifai et al., 2016; Silvério et al., 2019; Urquiza Muñoz et al., 2021), dynamics (Marra et al., 2018) and biogeochemical cycling (Espírito-Santo et al., 2014; dos Santos et al., 2016) where they occur.

Previous studies focusing on a more limited portion of the Amazon and fewer years of observation established that large-scale windthrows are rare events, with recurrence intervals of ∼27,000 years (eastern Amazon) to ∼90,000 years (western Amazon) (Espírito-Santo et al., 2014). While our results agree with long return intervals (>18,000 years) over most of the Amazon basin, for the ∼3% of the basin that experienced 2 (or more) events in the last 33 years over an area of 400 km^2 (corresponding to the darker contours in Figure 2a), return intervals are ∼1,000–2,700 years (examples in Figure 6). As our estimates of the damaged area are deliberately conservative

(Figure 3 suggests the damaged area could be ∼2–3 times larger depending on how we define it), return intervals could be of the order of hundreds to a thousand years in these regions. This time interval can be of the same order as the age of late successional trees (Vieira et al., 2005). Evidence for damage extending beyond the "core" windthrow region is supported by the observation that the passage of a strong squall-line causing severe windthrows near Manaus, Brazil in 2005 (Negrón-Juárez et al., 2010) also led to increased plot level wind-related mortality (Aleixo et al., 2019).

Quantifying the extent and impact of damage outside the core windthrow region is challenging but critical for evaluating the overall importance of this disturbance mechanism in Amazon. Previous attempts have fitted power law distributions to area-frequency data (Chambers et al., 2013; Espírito-Santo et al., 2014) to estimate damage at spatial scales smaller than can be confidently related to windthrows detected from Landsat imagery. Our results (Figures 5c and 5d) confirm those of Espírito-Santo et al. (2014) that a single power law distribution does not cover the entire size distribution from a few to thousands of hectares. While Espírito-Santo et al. (2014) found a break in slope at ∼10 ha in area, our data indicate slope changes between 30 and 100 ha, perhaps suggesting a transition from purely atmospheric impacts at larger spatial scales (where power laws might not be expected to apply), to power law distributions with varying slopes at smaller spatial scales, where forest characteristics have more impact on the damage experienced. Previous study demonstrate that distinct alpha values are necessary to achieve a satisfactory fit for mortality in both Manaus and Iquitos (Negrón-Juárez et al., 2018). Our study supports that a single power law alpha value is insufficient to explain the distribution of damage from windthrows across Amazon.

The selection of 30 ha as size threshold was made only to facilitate our basin-wide annual calculations. Previous studies employing the same methodology combined with field data have demonstrated the ability to identify gaps as small as 5 ha (Emmert et al., 2023; Negrón-Juárez et al., 2023) and even single Landsat pixels containing as few as eight downed trees (Negrón-Juárez et al., 2011). At the plot level, it has been shown that wind-induced tree mortality can account for up to 50% of overall tree mortality (Esquivel-Muelbert et al., 2020). These findings support that windthrows are an important mechanism of tree mortality not only in hotspot areas but across other regions as well. Future work is needed to understand whether windthrows affecting smaller areas are caused by different types of storms (e.g., associated microbursts) and whether/how these are related to the convective events associated with large downdrafts that can fell trees over tens to thousands of hectares.

As remote sensing is available at increasing spatial resolution, mapping of smaller windthrow events is potentially possible. However, detection and evaluation of the impact of windthrow on forest structure and function requires comparison with field observations of change in forest structure and biodiversity. Only a few field studies of recovery after large-scale wind damage are available (Emmert et al., 2023; Marra et al., 2018; Urquiza Muñoz et al., 2021). Existing forest inventories may not cover the full range of factors influencing landscape-to-regional variations in disturbance frequency, may not have sufficient spatial resolution to accurately capture small-scale disturbances (Gorgens et al., 2023; Simonetti et al., 2023), and are often conducted at discrete time intervals that may not coincide with the frequency of disturbance events (e.g., Aleixo et al., 2019).

The impact of wind on forest properties depends not only on the frequency, severity and area of damage, but also the rates of recovery of structure, species and functional composition (Gorgens et al., 2023; Silverio et al., 2019). Detailed studies of forest responses following windthrows in the Amazon are available only for two regions (Brazil and Peru), both in areas classified as disturbance "hotspots" in our analysis. These document how windthrow triggers secondary succession and controls patterns of forest diversity and dynamics by creating a mosaic of niches across the landscape (Figure 6) (Chambers et al., 2009; Marra et al., 2014; G. H. P. D. M. Ribeiro et al., 2014). Fallen trees and debris provide important resources for a wide range of organisms, including fungi, insects (Alencar et al., 2022; Bouget & Duelli, 2004), and small mammals. Dead wood and decaying organic matter resulting from dead trees contribute to nutrient cycling (dos Santos et al., 2016) and create habitats for specialized decomposers. While mortality of canopy trees that survived initial disturbance continues over subsequent years (Marra et al., 2018), new tree species including fast growing pioneers colonize the created gaps (Bordon et al., 2019; Marra et al., 2014; Ribeiro et al., 2014). This increased habitat heterogeneity supports a greater variety of species and can enhance overall ecosystem functioning (Lugo, 2008; Mitchell, 2013; Viljur et al., 2022).

Effects of windthrows on local carbon balance depend on the rate of decomposition of downed trees (Chambers et al., 2004), which takes up to several decades (Palace et al., 2012), compared to the rate of regrowth of new

biomass. In western Amazon (near Iquitos, Peru), biomass recovery to old-growth levels in windthrows ranging from 188 to 662 ha takes only ~20 years (Urquiza Muñoz et al., 2021). In central Amazon (near Manaus, Brazil), biomass recovery in windthrows ranging from 75 to 900 ha can take more than 40 years to recover to old-growth levels (Marra et al., 2018). However, the recovery of species and functional composition requires longer time intervals (Marra et al., 2018). Impacts of large windthrows on local to regional carbon balance will depend on the region surveyed, the degree to which there is damage to trees outside core windthrow areas, the time since disturbance, the successional stage of affected forests and the occurrence of additional and related mortality or damage (Silvério et al., 2019). Given the rapidity of decomposition and biomass accumulation, these effects will be most important in areas directly impacted.

Further investigation is needed to accurately identify and map windthrows smaller than 30 ha to assess their ecological importance (Chambers et al., 2013; Gorgens et al., 2023; Negrón-Juárez et al., 2018; Reis et al., 2022; Simonetti et al., 2023), especially as tree mortality at smaller spatial scales cannot be easily extrapolated from the spatial-temporal distribution of larger events (Espírito-Santo et al., 2014 and this study). Future studies can take advantage of increased resolution of satellite imagery to map windthrow damage on new windthrows (Emmert et al., 2023) and track their recovery trajectories. New remotes sensing products like LiDAR can identify canopy gaps at smaller spatial scales but do not specifically allow identification of the reason for gap formation, though broken or uprooted trees typically create larger gaps compared to standing dead trees (Esquivel-Muelbert et al., 2020; Reis et al., 2022; Simonetti et al., 2023). Future work comparing Lidar surveys with the locations of known large windthrows can help answer the question of how far damage associated with larger windthrow events extends beyond the core region detectable with confidence from the Landsat record and reported here. Such studies can also assess better the degree to which wind damage occurring at scales <30 ha are independent of, or related to, larger convective systems and topographic features. Detailed field surveys will also be necessary to improve estimates of tree mortality/damage and associated losses of biomass outside of the "core" damaged areas. Such studies would also contribute fundamental knowledge to understand the legacy of windthrows on evolutive processes such the relationships between wind disturbance and species distribution in tropical forests.

5. Conclusions

We presented the first annual analysis of windthrows in the Amazon for the period 1985–2020. Our results document an approximately four-fold increase in large (≥30 ha) windthrows per year associated with severe convective storms in the Amazon Basin over the 33 years documented. The increase in damage from convective storms felling large areas of forest in this region with sparse atmospheric time series adds to evidence documenting increases in extreme storms in other regions over the last decades. Windthrows tend to cluster in regions that coincide with metrics for meteorological conditions favoring convection in the central and western regions of the Amazon, and in these regions the mean size of windthrows is also larger. Overall, we detected no changes in the size distribution or severity of windthrows over the past 35 years, except for an increase in very large events (>500 ha) since 1990. Thus, it is the number of events that has increased. While we cannot attribute the cause for increase more specifically, our observations are consistent with reported changes in Amazon temperature and hydrometeorology over the same time period. We argue that the database of past windthrows we provide will be a valuable benchmark for testing cloud-resolving climate models that aim at providing a detailed explanation for the large observed increase in windthrows.

While across much of the Amazon basin, large-scale windthrows (≥30 ha) is sufficient to impact forest properties, especially forest structure and species composition, with roughly a third of the documented events occurring a ~3% of the Amazon basin with recurrence intervals of hundreds to thousands of years. The few studies of recovery following large windthrows indicate that while changes in species composition will last longer, biomass recovery can take only decades. Thus, carbon imbalances associated with large windthrows will be short-lived and difficult to measure at spatial scales larger than several hundred km^2. Further research is needed to understand wind damage at smaller spatial scales, and how or whether it is connected to larger convective systems creating windthrows we can detect with high confidence in Landsat records.

Given predictions of increased storm severity with global warming, the number of windthrows are also predicted to increase. This is likely to make wind disturbance a more important mechanism even outside the regions we have identified as most impacted, especially if large trees become more vulnerable to snapping and uprooting as a consequence of other emerging disturbances. The windthrow database we publish with this paper provides a

benchmark for evaluating future change in disturbance regimes. It also adds novel and valuable information for progress in atmospheric modeling, as well as field and remote sensing studies linking landscape and regional patterns of forest structure, dynamics and floristic composition across Amazon.

Conflict of Interest

The authors declare no conflicts of interest relevant to this study.

Data Availability Statement

All windthrows data are organized, structured, and stored in our Windthrow Inventory Database, Version 1.0 (WInD V.1) (Urquiza-Muñoz et al., 2024). Figures were made with R version 4.4.0 (R Core Team, 2022), R Studio version 2023.6.1.524 (RStudio Team, 2020), and QGIS version 3.34.6 (QGIS Development Team, 2009) available at https://posit.co/download/rstudio-desktop/ and https://qgis.org/download/ respectively. The platform Google earth engine (Gorelick et al., 2017) available at https://earthengine.google.com/ was used for access to Landsat 5 TM and Landsat 8 OLI images.

Acknowledgments

J.D.U.M. has been supported by the Max Planck Institute of Biogeochemistry, the German Academic Exchange Service (DAAD) as well as the International Max Planck Research School for Global Biogeochemical. D.M.M. and S.T. are supported by the ATTO Project funded by the German Federal Ministry of Education and Research (BMBF, contracts 01LB1001A and 01LK1602A), the Brazilian Ministério da Ciência, Tecnologia e Inovação (MCTI/FINEP contract 01.11.01248.00) and the Max Planck Society. S.T. and J. D.U.M also acknowledge support from the Balzan Foundation. R.N.J. is supported by the Next Generation Ecosystem Experiments-Tropics, and the Office of Science's Regional and Global Model Analysis of the US Department of Energy, Agreement Grant DE-AC02-05CH11231, and Reducing Uncertainties in Biogeochemical Interactions through Synthesis Computation Scientific Focus Area (RUBISCO SFA). M.V.P has been supported by Forest Data Connect of the National University of the Peruvian Amazon. The Windthrow Inventory Database (WInD V.1) is an innitiative from the research group Forest Functioning and Dynamics (ForFunDy: www.forfundy.com), led by J.D.U.M., S.T., and D.M.M. Open Access funding enabled and organized by Projekt DEAL.

References

Adams, J. (1995). Classification of multispectral images based on fractions of endmembers: Application to land-cover change in the Brazilian Amazon. *Remote Sensing of Environment*, *52*(2), 137–154. https://doi.org/10.1016/0034-4257(94)00098-8

Adams, J. B., & Gillespie, A. R. (2006). *Remote sensing of landscapes with spectral images: A physical modeling approach*. Cambridge University Press. https://doi.org/10.1017/CBO9780511617195

Aleixo, I., Norris, D., Hemerik, L., Barbosa, A., Prata, E., Costa, F., & Poorter, L. (2019). Amazonian rainforest tree mortality driven by climate and functional traits. *Nature Climate Change*, *9*(5), 384–388. https://doi.org/10.1038/s41558-019-0458-0

Alencar, J. B. R., Fonseca, C. R. V., Marra, D. M., & Baccaro, F. B. (2022). Windthrows promote higher diversity of saproxylic beetles (Coleoptera: Passalidae) in a Central Amazon forest. *Insect Conservation and Diversity*, *15*(1), 1–8. https://doi.org/10.1111/icad.12523

Araujo, R. F., Nelson, B. W., Celes, C. H. S., & Chambers, J. Q. (2017). Regional distribution of large blowdown patches across Amazonia in 2005 caused by a single convective squall line: Distribution of Amazonia Blowdown Damage. *Geophysical Research Letters*, *44*(15), 7793–7798. https://doi.org/10.1002/2017GL073564

Artaxo, P., Rizzo, L. V., Brito, J. F., Barbosa, H. M. J., Arana, A., Sena, E. T., et al. (2013). Atmospheric aerosols in Amazonia and land use change: From natural biogenic to biomass burning conditions. *Faraday Discussions*, *165*, 203. https://doi.org/10.1039/c3fd00052d

Attali, D., & Baker, C. (2023). ggExtra: Add marginal histograms to "ggplot2", and more "ggplot2" enhancements. Retrieved from https://CRAN.R-project.org/package=ggExtra

Bamston, A. G., Chelliah, M., & Goldenberg, S. B. (1997). Documentation of a highly ENSO-related SST region in the equatorial pacific: Research note. *Atmosphere-Ocean*, *35*(3), 367–383. https://doi.org/10.1080/07055900.1997.9649597

Barichivich, J., Gloor, E., Peylin, P., Brienen, R. J. W., Schöngart, J., Espinoza, J. C., & Pattnayak, K. C. (2018). Recent intensification of Amazon flooding extremes driven by strengthened Walker circulation. *Science Advances*, *4*(9), eaat8785. https://doi.org/10.1126/sciadv.aat8785

Bordon, N. G., Nogueira, A., Leal Filho, N., & Higuchi, N. (2019). Blowdown disturbance effect on the density, richness and species composition of the seed bank in Central Amazonia. *Forest Ecology and Management*, *453*, 117633. https://doi.org/10.1016/j.foreco.2019.117633

Bouget, C., & Duelli, P. (2004). The effects of windthrow on forest insect communities: A literature review. *Biological Conservation*, *118*(3), 281–299. https://doi.org/10.1016/j.biocon.2003.09.009

Caha, J. (2023). SpatialKDE: Kernel density estimation for spatial data [Computer Software]. https://jancaha.github.io/SpatialKDE/index.html and https://github.com/JanCaha/SpatialKDE

Cai, W., McPhaden, M. J., Grimm, A. M., Rodrigues, R. R., Taschetto, A. S., Garreaud, R. D., et al. (2020). Climate impacts of the El Niño–southern oscillation on south America. *Nature Reviews Earth & Environment*, *1*(4), 215–231. https://doi.org/10.1038/s43017-020-0040-3

Chambers, J. Q., Higuchi, N., Teixeira, L. M., Dos Santos, J., Laurance, S. G., & Trumbore, S. E. (2004). Response of tree biomass and wood litter to disturbance in a Central Amazon forest. *Oecologia*, *141*(4), 596–611. https://doi.org/10.1007/s00442-004-1676-2

Chambers, J. Q., Negrón-Juárez, R. I., Hurtt, G. C., Marra, D. M., & Higuchi, N. (2009). Lack of intermediate-scale disturbance data prevents robust extrapolation of plot-level tree mortality rates for old-growth tropical forests: Clustered gaps tropical tree mortality rates. *Ecology Letters*, *12*(12), E22–E25. https://doi.org/10.1111/j.1461-0248.2009.01398.x

Chambers, J. Q., Negron-Juarez, R. I., Marra, D. M., Di Vittorio, A., Tews, J., Roberts, D., et al. (2013). The steady-state mosaic of disturbance and succession across an old-growth Central Amazon forest landscape. *Proceedings of the National Academy of Sciences*, *110*(10), 3949–3954. https://doi.org/10.1073/pnas.1202894110

Chen, J., & Dai, A. (2023). The atmosphere has become increasingly unstable during 1979–2020 over the northern hemisphere. *Geophysical Research Letters*, *50*(20), e2023GL106125. https://doi.org/10.1029/2023GL106125

Dharani, M., & Sreenivasulu, G. (2021). Land use and land cover change detection by using principal component analysis and morphological operations in remote sensing applications. *International Journal of Computers and Applications*, *43*(5), 462–471. https://doi.org/10.1080/1206212X.2019.1578068

Diffenbaugh, N. S., Scherer, M., & Trapp, R. J. (2013). Robust increases in severe thunderstorm environments in response to greenhouse forcing. *Proceedings of the National Academy of Sciences*, *110*(41), 16361–16366. https://doi.org/10.1073/pnas.1307758110

dos Santos, L. T., Magnabosco Marra, D., Trumbore, S., de Camargo, P. B., Negrón-Juárez, R. I., Lima, A. J. N., et al. (2016). Windthrows increase soil carbon stocks in a central Amazon forest. *Biogeosciences*, *13*(4), 1299–1308. https://doi.org/10.5194/bg-13-1299-2016

Emmert, L., Negrón-Juárez, R. I., Chambers, J. Q., Santos, J. D., Lima, A. J. N., Trumbore, S., & Marra, D. M. (2023). Sensitivity of optical satellites to estimate windthrow tree-mortality in a central Amazon forest [Preprint]. *Environmental Earth Sciences*. https://doi.org/10.20944/preprints202305.1631.v1

Espinoza, J. C., Marengo, J. A., Schongart, J., & Jimenez, J. C. (2022). The new historical flood of 2021 in the Amazon River compared to major floods of the 21st century: Atmospheric features in the context of the intensification of floods. *Weather and Climate Extremes*, *35*, 100406. https://doi.org/10.1016/j.wace.2021.100406

Espinoza, J. C., Ronchail, J., Marengo, J. A., & Segura, H. (2019). Contrasting North–South changes in Amazon wet-day and dry-day frequency and related atmospheric features (1981–2017). *Climate Dynamics*, *52*(9–10), 5413–5430. https://doi.org/10.1007/s00382-018-4462-2

Espírito-Santo, F. D. B., Gloor, M., Keller, M., Malhi, Y., Saatchi, S., Nelson, B., et al. (2014). Size and frequency of natural forest disturbances and the Amazon forest carbon balance. *Nature Communications*, *5*(1), 3434. https://doi.org/10.1038/ncomms4434

Esquivel-Muelbert, A., Phillips, O. L., Brienen, R. J. W., Fauset, S., Sullivan, M. J. P., Baker, T. R., et al. (2020). Tree mode of death and mortality risk factors across Amazon forests. *Nature Communications*, *11*(1), 5515. https://doi.org/10.1038/s41467-020-18996-3

Feng, Y., Negrón-Juárez, R., Chiang, J. C. H., & Chambers, J. Q. (2023). Case studies of forest windthrows and mesoscale convective systems in Amazonia. *Geophysical Research Letters*, *50*(12), e2023GL104395. https://doi.org/10.1029/2023GL104395

Feng, Y., Negrón-Juárez, R. I., Romps, D. M., & Chambers, J. Q. (2023). Amazon windthrow disturbances are likely to increase with storm frequency under global warming. *Nature Communications*, *14*(1), 101. https://doi.org/10.1038/s41467-022-35570-1

Feng, Z., Leung, L. R., Hardin, J., Terai, C. R., Song, F., & Caldwell, P. (2023). Mesoscale convective systems in DYAMOND global convection-permitting simulations. *Geophysical Research Letters*, *50*(4), e2022GL102603. https://doi.org/10.1029/2022GL102603

Foga, S., Scaramuzza, P. L., Guo, S., Zhu, Z., Dilley, R. D., Beckmann, T., et al. (2017). Cloud detection algorithm comparison and validation for operational Landsat data products. *Remote Sensing of Environment*, *194*, 379–390. https://doi.org/10.1016/j.rse.2017.03.026

Fujita, T. (1990). DOWNBURSTS: Meteorological features and wind field characteristics. *Journal of Wind Engineering and Industrial Aerodynamics*, *36*(1–3), 75–86. https://doi.org/10.1016/0167-6105(90)90357-i

Garg, P. K. (2020). Effect of contamination and adjacency factors on snow using spectroradiometer and hyperspectral images. In P. C. Pandey, P. K. Srivastava, H. Balzter, B. Bhattacharya, & G. P. Petropoulos (Eds.), *Hyperspectral remote sensing* (pp. 167–196). Elsevier. https://doi.org/10.1016/B978-0-08-102894-0.00016-4

Garstang, M., White, S., Shugart, H. H., & Halverson, J. (1998). Convective cloud downdrafts as the cause of large blowdowns in the Amazon rainforest. *Meteorology and Atmospheric Physics*, *67*(1–4), 199–212. https://doi.org/10.1007/BF01277510

Gloor, M., Brienen, R. J. W., Galbraith, D., Feldpausch, T. R., Schöngart, J., Guyot, J.-L., et al. (2013). Intensification of the Amazon hydrological cycle over the last two decades. *Geophysical Research Letters*, *40*(9), 1729–1733. https://doi.org/10.1002/grl.50377

Gombin, J., Vaidyanathan, R., & Agafonkin, V. (2020). Concaveman: A very fast 2D Concave Hull algorithm. Retrieved from https://CRAN.R-project.org/package=concaveman

Gorelick, N., Hancher, M., Dixon, M., Ilyushchenko, S., Thau, D., & Moore, R. (2017). Google earth engine: Planetary-scale geospatial analysis for everyone. *Remote Sensing of Environment*, *202*, 18–27. https://doi.org/10.1016/j.rse.2017.06.031

Gorgens, E. B., Keller, M., Jackson, T., Marra, D. M., Reis, C. R., De Almeida, D. R. A., et al. (2023). Out of steady state: Tracking canopy gap dynamics across Brazilian Amazon. *Biotropica*, *55*(4), 13226–13766. https://doi.org/10.1111/btp.13226

Hansen, M. C., Potapov, P. V., Moore, R., Hancher, M., Turubanova, S. A., Tyukavina, A., et al. (2013). High-resolution global maps of 21st-century forest cover change. *Science*, *342*(6160), 850–853. https://doi.org/10.1126/science.1244693

Huang, B., Thorne, P. W., Banzon, V. F., Boyer, T., Chepurin, G., Lawrimore, J. H., et al. (2017). Extended reconstructed sea surface temperature, version 5 (ERSSTv5): Upgrades, validations, and intercomparisons. *Journal of Climate*, *30*(20), 8179–8205. https://doi.org/10.1175/JCLI-D-16-0836.1

Lugo, A. E. (2008). Visible and invisible effects of hurricanes on forest ecosystems: An international review. *Austral Ecology*, *33*(4), 368–398. https://doi.org/10.1111/j.1442-9993.2008.01894.x

Marengo, J. A. (2004). Interdecadal variability and trends of rainfall across the Amazon basin. *Theoretical and Applied Climatology*, *78*(1–3). https://doi.org/10.1007/s00704-004-0045-8

Marengo, J. A., Souza, C. M., Thonicke, K., Burton, C., Halladay, K., Betts, R. A., et al. (2018). Changes in climate and land use over the Amazon region: Current and future variability and trends. *Frontiers in Earth Science*, *6*, 228. https://doi.org/10.3389/feart.2018.00228

Marra, D. M., Chambers, J. Q., Higuchi, N., Trumbore, S. E., Ribeiro, G. H. P. M., dos Santos, J., et al. (2014). Large-scale wind disturbances promote tree diversity in a central Amazon forest. *PLoS One*, *9*(8), e103711. https://doi.org/10.1371/journal.pone.0103711

Marra, D. M., Trumbore, S. E., Higuchi, N., Ribeiro, G. H. P. M., Negrón-Juárez, R. I., Holzwarth, F., et al. (2018). Windthrows control biomass patterns and functional composition of Amazon forests. *Global Change Biology*, *24*(12), 5867–5881. https://doi.org/10.1111/gcb.14457

Mendonça, A. C. S., Dias-Júnior, C. Q., Acevedo, O. C., Santana, R. A., Costa, F. D., Negrón-Juarez, R. I., et al. (2023). Turbulence regimes in the nocturnal roughness sublayer: Interaction with deep convection and tree mortality in the Amazon. *Agricultural and Forest Meteorology*, *339*, 109526. https://doi.org/10.1016/j.agrformet.2023.109526

Mitchell, S. J. (2013). Wind as a natural disturbance agent in forests: A synthesis. *Forestry*, *86*(2), 147–157. https://doi.org/10.1093/forestry/cps058

Moss, J. (2019). univariateML: An R package for maximum likelihood estimation of univariate densities. *Journal of Open Source Software*, *4*(44), 1863. https://doi.org/10.21105/joss.01863

Negrón-Juárez, R., Chambers, J. Q., Guimaraes, G., Zeng, H., Raupp, C. F. M., Marra, D. M., et al. (2010). Widespread Amazon forest tree mortality from a single cross-basin squall line event: WIND-DRIVEN tree mortality in Amazonia. *Geophysical Research Letters*, *37*(16). https://doi.org/10.1029/2010GL043733

Negrón-Juárez, R., Chambers, J. Q., Marra, D. M., Ribeiro, G. H. P. M., Rifai, S. W., Higuchi, N., & Roberts, D. (2011). Detection of subpixel treefall gaps with Landsat imagery in Central Amazon forests. *Remote Sensing of Environment*, *115*(12), 3322–3328. https://doi.org/10.1016/j.rse.2011.07.015

Negrón-Juárez, R., Holm, J. A., Faybishenko, B., Magnabosco-Marra, D., Fisher, R. A., Shuman, J. K., et al. (2020). Landsat near-infrared (NIR) band and ELM-FATES sensitivity to forest disturbances and regrowth in the Central Amazon. *Biogeosciences*, *17*(23), 6185–6205. https://doi.org/10.5194/bg-17-6185-2020

Negrón-Juárez, R., Holm, J. A., Marra, D. M., Rifai, S. W., Riley, W. J., Chambers, J. Q., et al. (2018). Vulnerability of Amazon forests to storm-driven tree mortality. *Environmental Research Letters*, *13*(5), 054021. https://doi.org/10.1088/1748-9326/aabe9f

Negrón-Juárez, R., Jenkins, H., Raupp, C., Riley, W., Kueppers, L., Magnabosco Marra, D., et al. (2017). Windthrow variability in central Amazonia. *Atmosphere*, *8*(12), 28. https://doi.org/10.3390/atmos8020028

Negrón-Juárez, R., Koven, C. D., Riley, W. J., Knox, R. G., & Chambers, J. Q. (2015). Observed allocations of productivity and biomass, and turnover times in tropical forests are not accurately represented in CMIP5 Earth system models. *Environmental Research Letters*, *10*(6), 064017. https://doi.org/10.1088/1748-9326/10/6/064017

Negrón-Juárez, R., Magnabosco-Marra, D., Feng, Y., Urquiza-Muñoz, J. D., Riley, W. J., & Chambers, J. Q. (2023). Windthrow characteristics and their regional association with rainfall, soil, and surface elevation in the Amazon. *Environmental Research Letters*, *18*(1), 014030. https://doi.org/10.1088/1748-9326/acaf10

Negron-Juarez, R., Wehner, M., Silva Dias, M. A. F., Ullrich, P., Chambers, J., & Riley, W. J. (2024). Coupled model intercomparison Project phase 6 (CMIP6) high resolution model intercomparison Project (HighResMIP) bias in extreme rainfall drives underestimation of Amazonian precipitation. *Environmental Research Communications*, *6*(9), 091001. https://doi.org/10.1088/2515-7620/ad6ff9

Nelson, B., & Amaral, I. (1994). Destructive wind effects detected in TM image in the Amazon basin. In *Proceedings of the international society for photogrammetry and remote sensing* (pp. 339–343).

Nelson, B., Kapos, V., Adams, J. B., Oliveira, W. J., & Braun, O. P. G. (1994). Forest disturbance by large blowdowns in the Brazilian Amazon. *Ecology*, *75*(3), 853–858. https://doi.org/10.2307/1941742

Palace, M., Keller, M., Hurtt, G., & Frolking, S. (2012). A review of above ground Necromass in tropical forests. In P. Sudarshana (Ed.), *Tropical forests*. InTech. https://doi.org/10.5772/33085

Pekel, J.-F., Cottam, A., Gorelick, N., & Belward, A. S. (2016). High-resolution mapping of global surface water and its long-term changes. *Nature*, *540*(7633), 418–422. https://doi.org/10.1038/nature20584

Peterson, C. J., Ribeiro, G. H. P. D. M., Negrón-Juárez, R., Marra, D. M., Chambers, J. Q., Higuchi, N., et al. (2019). Critical wind speeds suggest wind could be an important disturbance agent in Amazonian forests. *Forestry: International Journal of Financial Research*, *92*(4), 444–459. https://doi.org/10.1093/forestry/cpz025

Prein, A. F. (2023). Thunderstorm straight line winds intensify with climate change. *Nature Climate Change*, *13*(12), 1353–1359. https://doi.org/10.1038/s41558-023-01852-9

QGIS Development Team. (2009). QGIS geographic information system [Computer software]. *Open Source Geospatial Foundation*. http://qgis.osgeo.org

Rasmussen, K. L., Prein, A. F., Rasmussen, R. M., Ikeda, K., & Liu, C. (2020). Changes in the convective population and thermodynamic environments in convection-permitting regional climate simulations over the United States. *Climate Dynamics*, *55*(1–2), 383–408. https://doi.org/10.1007/s00382-017-4000-7

R Core Team. (2022). R: A language and environment for statistical computing [Computer software]. *R Foundation for Statistical Computing*. http://www.R-project.org/

Rehbein, A., & Ambrizzi, T. (2023). Mesoscale convective systems over the Amazon basin in a changing climate under global warming. *Climate Dynamics*, *61*(3–4), 1815–1827. https://doi.org/10.1007/s00382-022-06657-8

Reis, C. R., Jackson, T. D., Gorgens, E. B., Dalagnol, R., Jucker, T., Nunes, M. H., et al. (2022). Forest disturbance and growth processes are reflected in the geographical distribution of large canopy gaps across the Brazilian Amazon. *Journal of Ecology*, *110*(12), 2971–2983. https://doi.org/10.1111/1365-2745.14003

Ribeiro, G. H. P. D. M., Suwa, R., Marra, D. M., Lima, A. J. N., Kajimoto, T., Ishizuka, M., & Higuchi, N. (2014). Allometry for Juvenile trees in an Amazonian forest after wind disturbance. *Japan Agricultural Research Quarterly: Japan Agricultural Research Quarterly*, *48*(2), 213–219. https://doi.org/10.6090/jarq.48.213

Ribeiro, G. H. P. M., Chambers, J. Q., Peterson, C. J., Trumbore, S. E., Magnabosco Marra, D., Wirth, C., et al. (2016). Mechanical vulnerability and resistance to snapping and uprooting for Central Amazon tree species. *Forest Ecology and Management*, *380*, 1–10. https://doi.org/10.1016/j.foreco.2016.08.039

Riemann-Campe, K., Fraedrich, K., & Lunkeit, F. (2009). Global climatology of convective available potential energy (CAPE) and convective Inhibition (CIN) in ERA-40 reanalysis. *Atmospheric Research*, *93*(1–3), 534–545. https://doi.org/10.1016/j.atmosres.2008.09.037

Rifai, S. W., Urquiza Muñoz, J. D., Negrón-Juárez, R. I., Ramírez Arévalo, F. R., Tello-Espinoza, R., Vanderwel, M. C., et al. (2016). Landscape-scale consequences of differential tree mortality from catastrophic wind disturbance in the Amazon. *Ecological Applications*, *26*(7), 2225–2237. https://doi.org/10.1002/eap.1368

Roberts, D. A., Gardner, M., Church, R., Ustin, S., Scheer, G., & Green, R. O. (1998). Mapping Chaparral in the Santa Monica Mountains using multiple endmember spectral mixture models. *Remote Sensing of Environment*, *65*(3), 267–279. https://doi.org/10.1016/S0034-4257(98)00037-6

RStudio Team. (2020). RStudio: Integrated Development for R [Computer Software]. *RStudio*. http://www.rstudio.com/

Satoh, M., Stevens, B., Judt, F., Khairoutdinov, M., Lin, S.-J., Putman, W. M., & Düben, P. (2019). Global cloud-resolving models. *Current Climate Change Reports*, *5*(3), 172–184. https://doi.org/10.1007/s40641-019-00131-0

Schumacher, R. S., & Rasmussen, K. L. (2020). The formation, character and changing nature of mesoscale convective systems. *Nature Reviews Earth & Environment*, *1*(6), 300–314. https://doi.org/10.1038/s43017-020-0057-7

Seeley, J. T., & Romps, D. M. (2015). Why does tropical convective available potential energy (CAPE) increase with warming? *Geophysical Research Letters*, *42*(23). https://doi.org/10.1002/2015GL066199

Silvério, D. V., Brando, P. M., Bustamante, M. M. C., Putz, F. E., Marra, D. M., Levick, S. R., & Trumbore, S. E. (2019). Fire, fragmentation, and windstorms: A recipe for tropical forest degradation. *Journal of Ecology*, *107*(2), 656–667. https://doi.org/10.1111/1365-2745.13076

Simonetti, A., Araujo, R. F., Celes, C. H. S., Da Silva E Silva, F. R., Dos Santos, J., Higuchi, N., et al. (2023). Canopy gaps and associated losses of biomass – Combining UAV imagery and field data in a central Amazon forest. *Biogeosciences*, *20*(17), 3651–3666. https://doi.org/10.5194/bg-20-3651-2023

Singh, M. S., Kuang, Z., Maloney, E. D., Hannah, W. M., & Wolding, B. O. (2017). Increasing potential for intense tropical and subtropical thunderstorms under global warming. *Proceedings of the National Academy of Sciences*, *114*(44), 11657–11662. https://doi.org/10.1073/pnas.1707603114

Stoica, P., & Selen, Y. (2004). Model-order selection. *IEEE Signal Processing Magazine*, *21*(4), 36–47. https://doi.org/10.1109/MSP.2004.1311138

Tai, S., Feng, Z., Ma, P., Schumacher, C., & Fast, J. D. (2021). Representations of precipitation diurnal cycle in the Amazon as simulated by observationally constrained cloud-system resolving and global climate models. *Journal of Advances in Modeling Earth Systems*, *13*(11), e2021MS002586. https://doi.org/10.1029/2021MS002586

Urquiza Muñoz, J. D., Magnabosco Marra, D., Negrón-Juarez, R. I., Tello-Espinoza, R., Alegría-Muñoz, W., Pacheco-Gómez, T., et al. (2021). Recovery of forest structure following large-scale windthrows in the northwestern Amazon. *Forests*, *12*(6), 667. https://doi.org/10.3390/f12060667

Urquiza-Muñoz, J. D., Negrón-Juarez, R. I., Trumbore, S., Brenning, A., Vasquez Parana, C. M., Tello-Espinoza, R., et al. (2024). Windthrows inventory data base (WInD) (version 1) [Dataset]. *Zenodo*. https://doi.org/10.5281/ZENODO.11168104

Vieira, S., Trumbore, S., Camargo, P. B., Selhorst, D., Chambers, J. Q., Higuchi, N., & Martinelli, L. A. (2005). Slow growth rates of Amazonian trees: Consequences for carbon cycling. *Proceedings of the National Academy of Sciences*, *102*(51), 18502–18507. https://doi.org/10.1073/pnas.0505966102

Viljur, M., Abella, S. R., Adámek, M., Alencar, J. B. R., Barber, N. A., Beudert, B., et al. (2022). The effect of natural disturbances on forest biodiversity: An ecological synthesis. *Biological Reviews*, *97*(5), 1930–1947. https://doi.org/10.1111/brv.12876

Windmiller, J. M., Bao, J., Sherwood, S. C., Schanzer, T. D., & Fuchs, D. (2023). Predicting convective downdrafts from updrafts and environmental conditions in a global storm resolving simulation. *Journal of Advances in Modeling Earth Systems*, *15*(3), e2022MS003048. https://doi.org/10.1029/2022MS003048

Yoon, J.-H., & Zeng, N. (2010). An Atlantic influence on Amazon rainfall. *Climate Dynamics*, *34*(2–3), 249–264. https://doi.org/10.1007/s00382-009-0551-6